THE SPATIAL SUB-SEPARATION OF STRANGENESS FROM ANTI-STRANGENESS IN RHICs

L. Bravina, O. Panova, O. Vitiuk,

E. Zabrodin and H. Stoecker

SQM2019, 10-15.06.2019, Bari, Italy

Outline

I. Motivation
II. Thermalization in relativistic heavy-ion collisions. Statistical model of ideal hadron gas
III. Strangeness in the central cell
IV. Freeze-out (dN/dt) of main hadron species
V. Spatial separation of S from anti-S :
  - in Thermal model predictions of Yields
  - directed flow for different particles
  - in lambda-antilambda polarization
VI. Conclusions

Dynamic Regimes

Parton distribution,
Nuclear geometry
Nuclear shadowing

Parton production &
regeneration
(or, sQGP)

Chemical freeze-out
(Quark recombination)

Jet fragmentation
functions

Hadron rescattering

Thermal freeze-out

Hadron decays

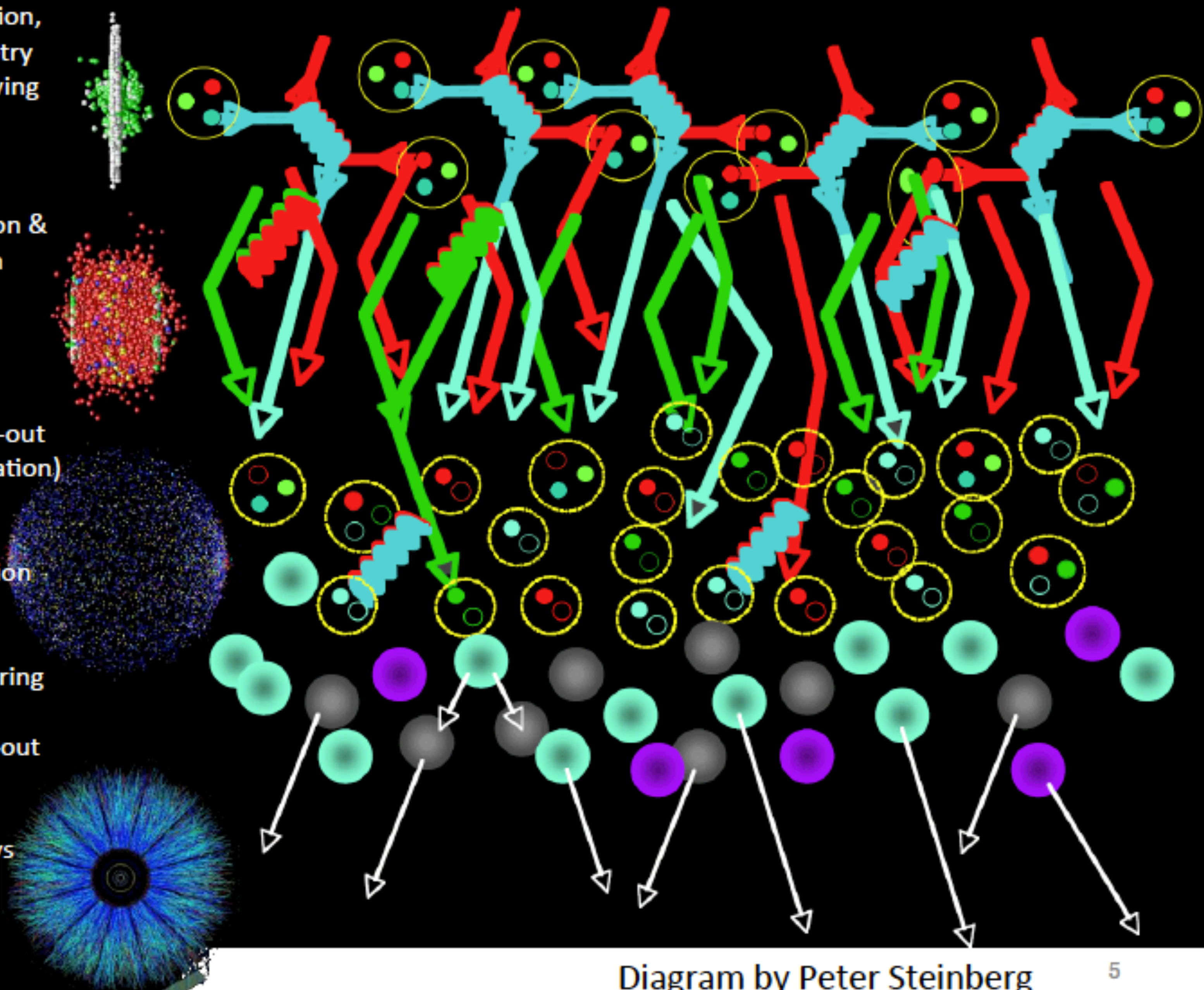

Diagram by Peter Steinberg

Motivation

Au+Au at $E_{lab} = 40$A GeV and $b = 0$ fm within UrQMD

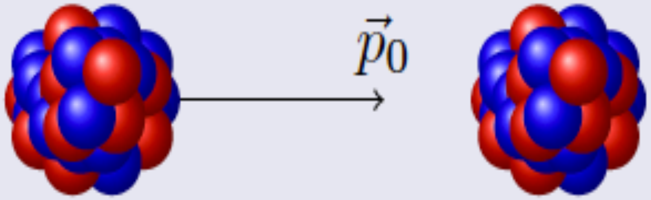

- To do the analysis of the spatio-temporal evolution of all particles in the $T - \mu_B$, $T - \mu_S$ plane and the analysis of the finally emitted particles in $x - t$ plane.
- See the spatial separation of strange particles from non strange (and of mesons from baryons).
- Find average T, μ_B, μ_S of different particles at freeze-out time.

Identified hadron yields

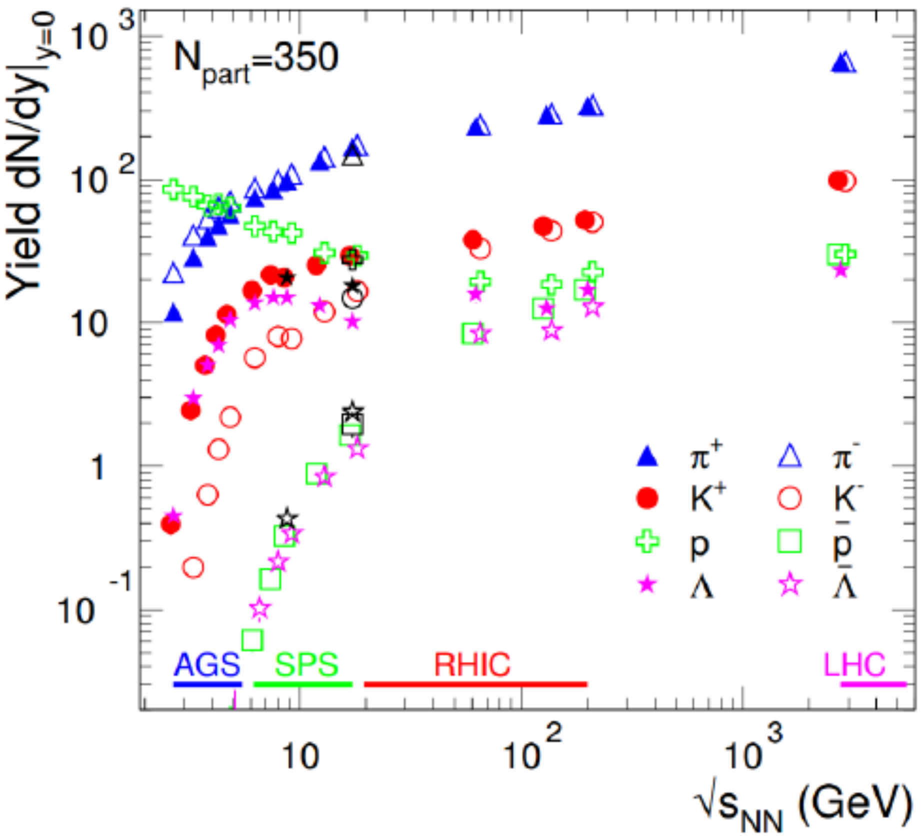

- Lots of particles, most newly created from the excited gluon fields ($E=mc^2$)
- Large variety of species:
  $\pi^{\pm}(u\bar{d},d\bar{u})$, m=140 MeV
  $K^{\pm}(u\bar{s},s\bar{u})$, m=494 MeV
  p(uud), m=938 MeV
  Λ(uds), m=1116 MeV
  also: Ξ(dss), Ω(sss), …
- Abundancies follow mass hierarchy, except at low energies where remnants from the incoming nuclei are significant
- What do we learn?

Grand Canonical Ensemble

$$\ln Z_i = \frac{V g_i}{2\pi^2} \int_0^\infty \pm p^2 dp \ln(1 \pm \exp(-(E_i - \mu_i)/T))$$

$$n_i = N/V = -\frac{T}{V}\frac{\partial \ln Z_i}{\partial \mu} = \frac{g_i}{2\pi^2} \int_0^\infty \frac{p^2 \, \mathrm{d}p}{\exp((E_i - \mu_i)/T) \pm 1}$$

$$\mu_i = \mu_B B_i + \mu_S S_i + \mu_{I_3} I_i^3$$

Fit at each energy provides values for T and μ_b

for every conserved quantum number there is a chemical potential μ
but can use conservation laws to constrain:

- Baryon number: $V \sum_i n_i B_i = Z + N$ $\rightarrow V$
- Strangeness: $V \sum_i n_i S_i = 0$ $\rightarrow \mu_S$
- Charge: $V \sum_i n_i I_i^3 = \frac{Z - N}{2}$ $\rightarrow \mu_{I_3}$

This leaves only μ_b and T as free parameter when 4π considered

for rapidity slice fix volume e.g. by dN_{ch}/dy

Chemical freeze-out

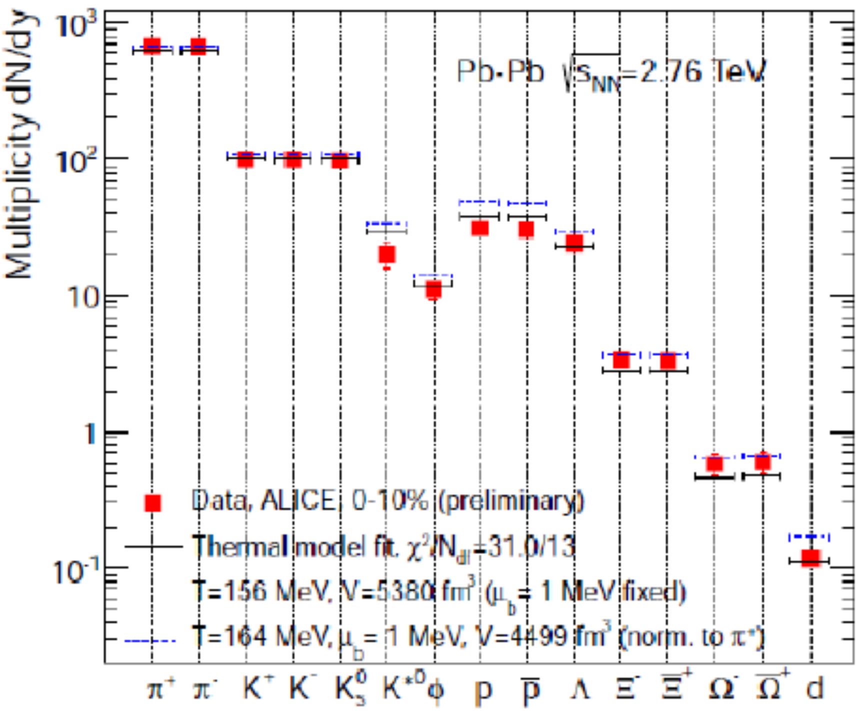

- Thermal fits of hadron abundancies:

$$n_i = N_i/V = -\frac{T}{V}\frac{\partial \ln Z_i}{\partial \mu} = \frac{g_i}{2\pi^2}\int_0^\infty \frac{p^2 dp}{\exp[(E_i-\mu_i)/T]\pm 1}$$

- Quantum numbers conservation

$\mu=\mu_B B+\mu_{I3} I_3+\mu_S S+\mu_C C$

- Hadron yields N_i can be obtained using only 3 parameters: (T_{chem},μ_B, V)
- The hadron abundancies are in agreement with a thermally equilibrated system

T_{chem}=155-165 MeV

μ_B~0

Central cell:
Relaxation to (local) equilibrium

Equilibration in the Central Cell

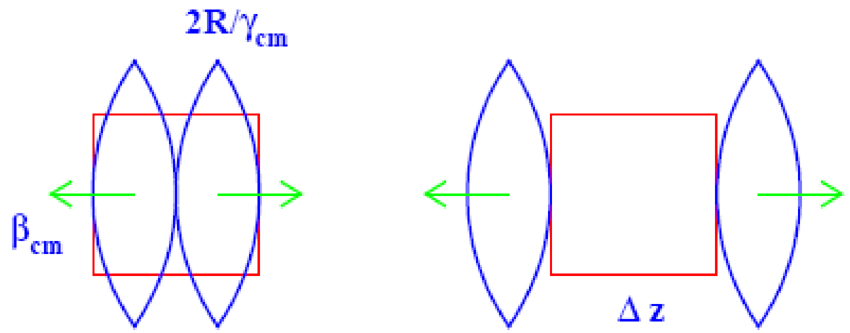

$t^{cross} = 2R/(\gamma_{cm}\,\beta_{cm})$ $\qquad$ $t^{eq} \geq t^{cross} + \Delta z/(2\beta_{cm})$

Kinetic equilibrium:

Isotropy of velocity distributions

Isotropy of pressure

Thermal equilibrium:

Energy spectra of particles are described by Boltzmann distribution

L.Bravina et al., PLB 434 (1998) 379; JPG 25 (1999) 351

$$\frac{dN_i}{4\pi p E dE} = \frac{V g_i}{(2\pi\hbar)^3} \exp\left(\frac{\mu_i}{T}\right) \exp\left(-\frac{E_i}{T}\right)$$

Chemical equlibrium:

Particle yields are reproduced by SM with the same values of $(T,\ \mu_B,\ \mu_S)$:

$$N_i = \frac{V g_i}{2\pi^2\hbar^3} \int_0^\infty p^2 dp \exp\left(\frac{\mu_i}{T}\right) \exp\left(-\frac{E_i}{T}\right)$$

Statistical model of ideal hadron gas

input values

output values

$$\varepsilon^{\rm mic} = \frac{1}{V}\sum_i E_i^{\rm SM}(T,\mu_{\rm B},\mu_{\rm S}),$$

$$\rho_{\rm B}^{\rm mic} = \frac{1}{V}\sum_i B_i \cdot N_i^{\rm SM}(T,\mu_{\rm B},\mu_{\rm S}),$$

$$\rho_{\rm S}^{\rm mic} = \frac{1}{V}\sum_i S_i \cdot N_i^{\rm SM}(T,\mu_{\rm B},\mu_{\rm S}).$$

Multiplicity

$$N_i^{\rm SM} = \frac{V g_i}{2\pi^2\hbar^3}\int_0^\infty p^2 f(p,m_i)dp,$$

Energy

$$E_i^{\rm SM} = \frac{V g_i}{2\pi^2\hbar^3}\int_0^\infty p^2 \sqrt{p^2+m_i^2}\, f(p,m_i)dp$$

Pressure

$$P^{\rm SM} = \sum_i \frac{g_i}{2\pi^2\hbar^3}\int_0^\infty p^2 \frac{p^2}{3(p^2+m_i^2)^{1/2}}\, f(p,m_i)dp$$

Entropy density

$$s^{\rm SM} = -\sum_i \frac{g_i}{2\pi^2\hbar^3}\int_0^\infty f(p,m_i)\,\left[\ln f(p,m_i)-1\right]\,p^2dp$$

Kinetic Equilibrium

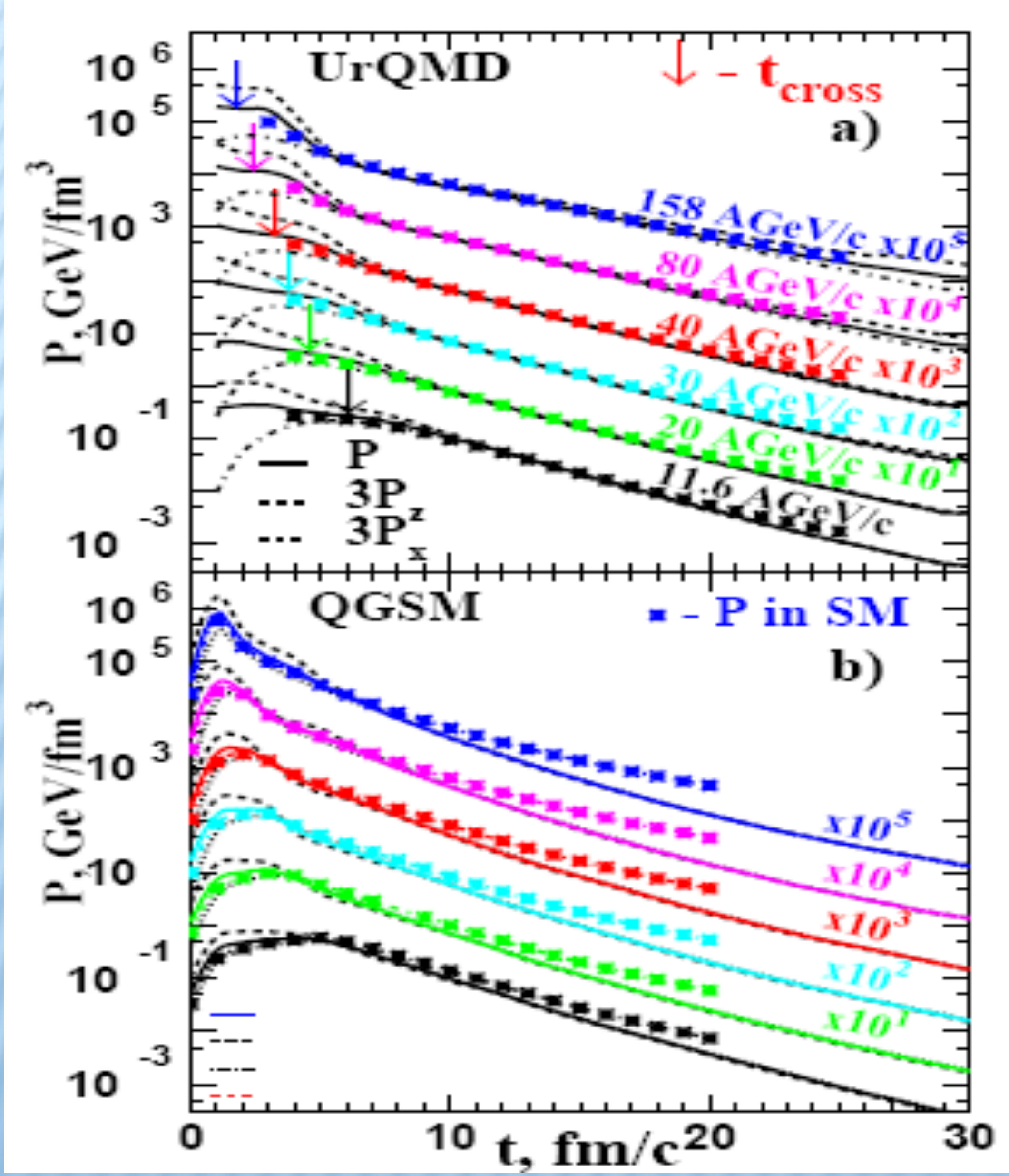

Isotropy of pressure

L.Bravina et al., PRC 78 (2008) 014907

Pressure becomes isotropic for all energies from 11.6 AGeV to 158 AGeV

NEGATIVE NET STRANGENESS DENSITY

Net strangeness density in the central cell at 11 to 80 AGeV

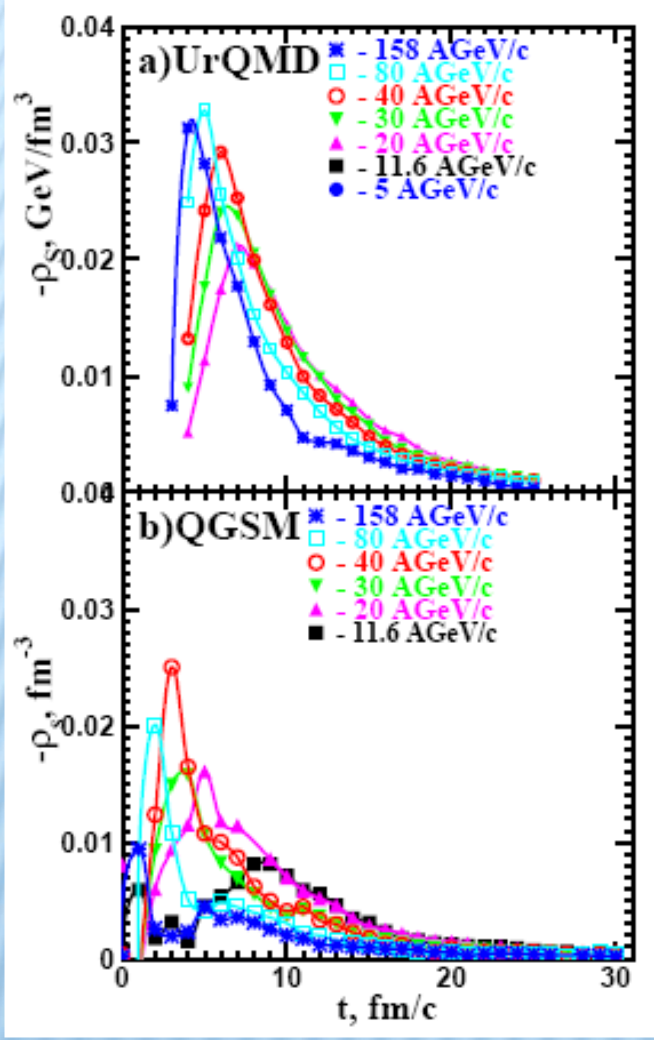

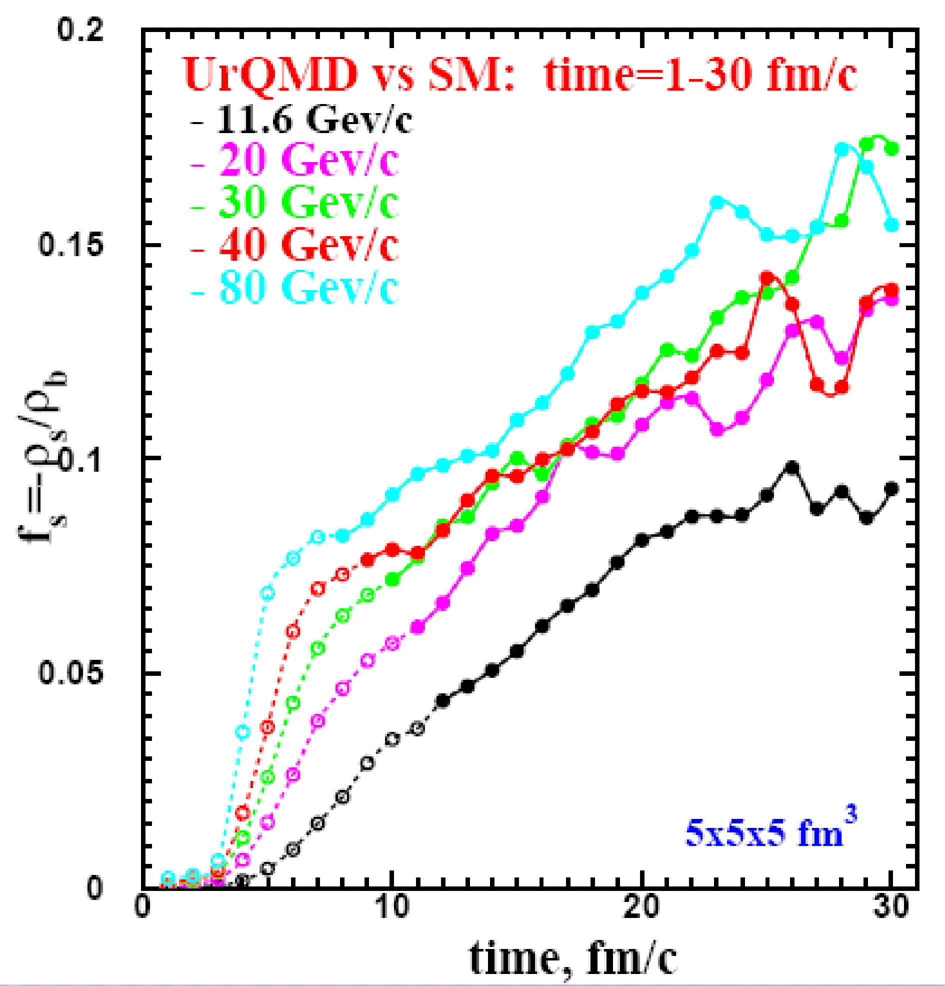

Net strangeness in the cell is negative because of different interaction cross sections for Kaons and antiKaons with Baryons

THERMAL AND CHEMICAL EQUILIBRIUM

Boltzmann fit to the energy spectra

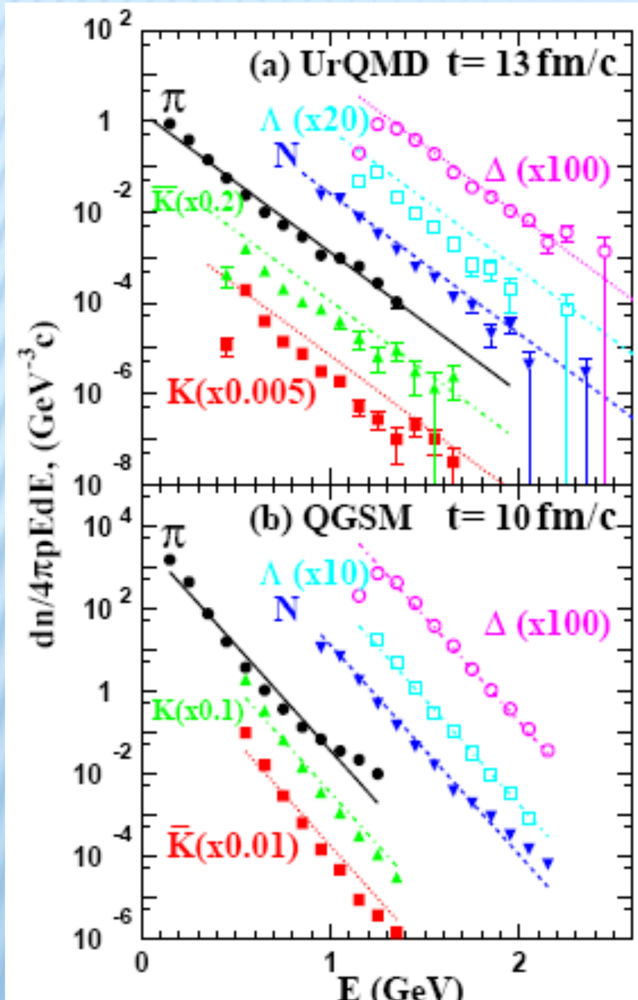

PRC 78 (2008) 014907

Particle yields

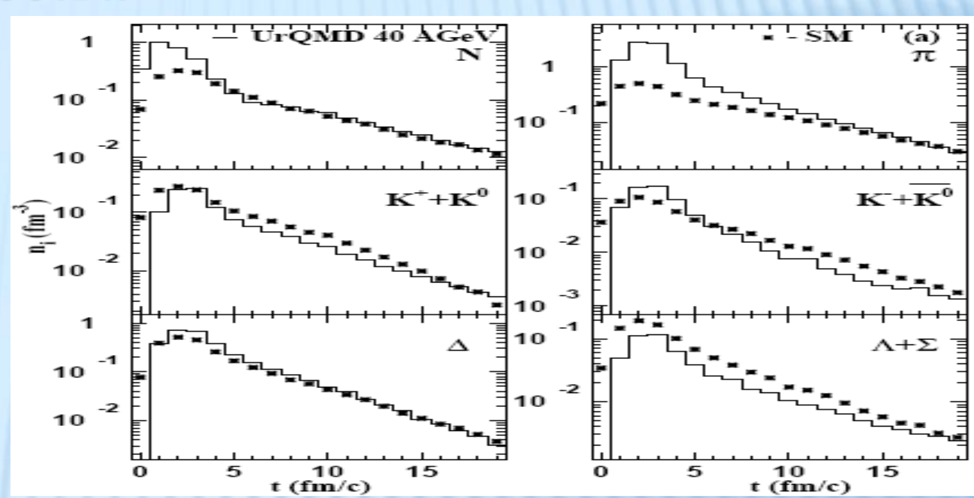

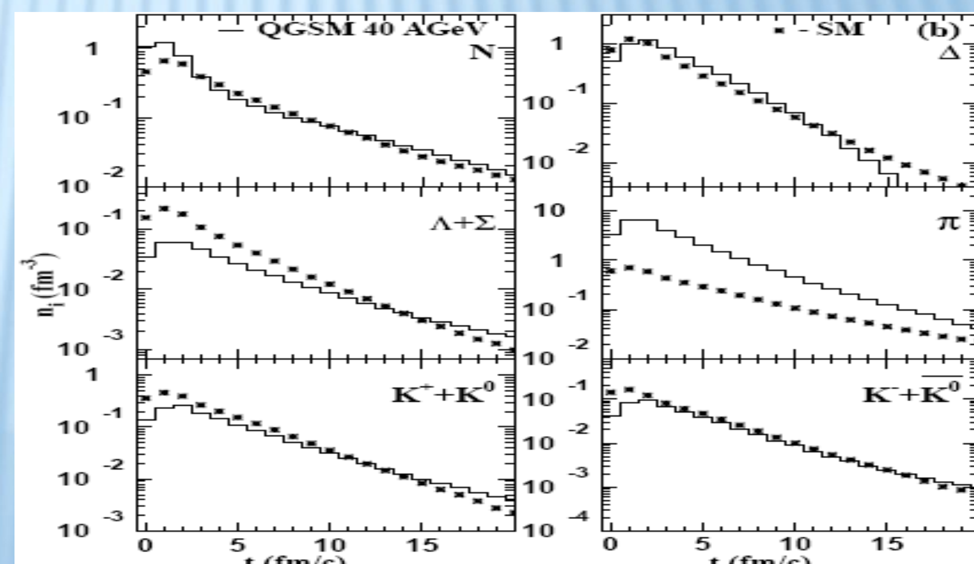

Thermal and chemical equilibrium seems to be reached

HOW DENSE CAN BE THE MEDIUM?

PRC 78 (2008) 014907

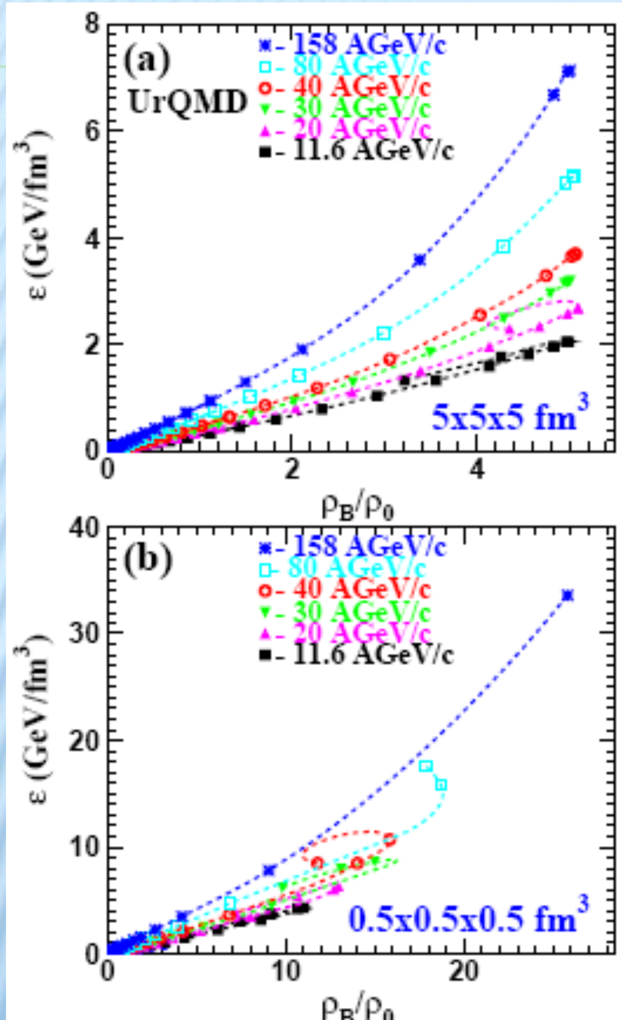

"Big" cell (V = 5x5x5 fm^3)

"Small" cell (V => 0)

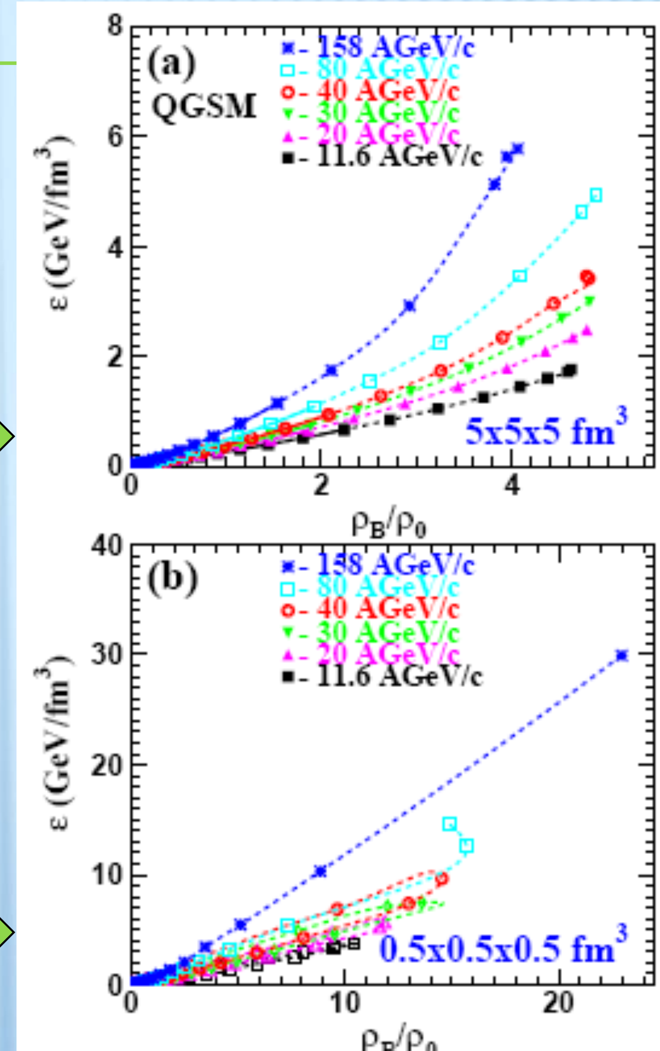

Dramatic differences at the non-equilibrium stage; after beginning of kinetic equilibrium the energy densities and the baryon densities are the same for "small" and "big" cell

COMPARISON BETWEEN MODELS

The phase trajectories at the center of a head-on Au+Au collisions

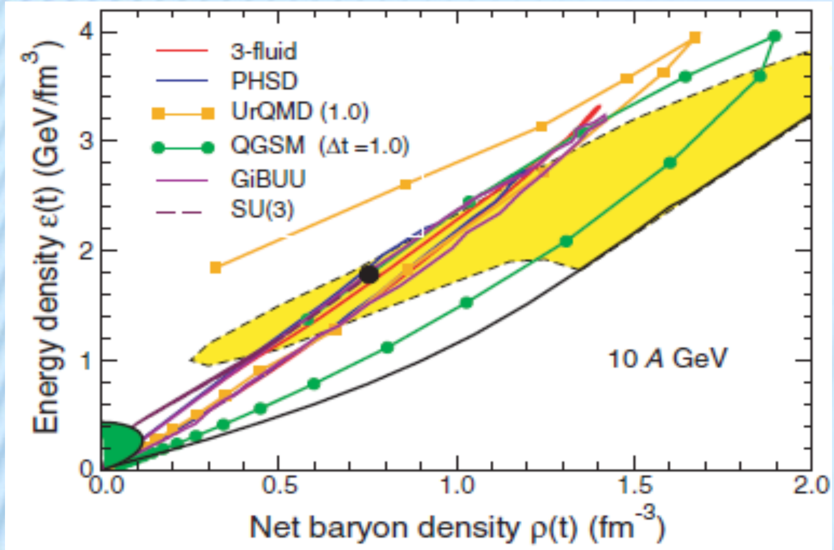

I. Arsene et al., PRC 75 (2007) 034902

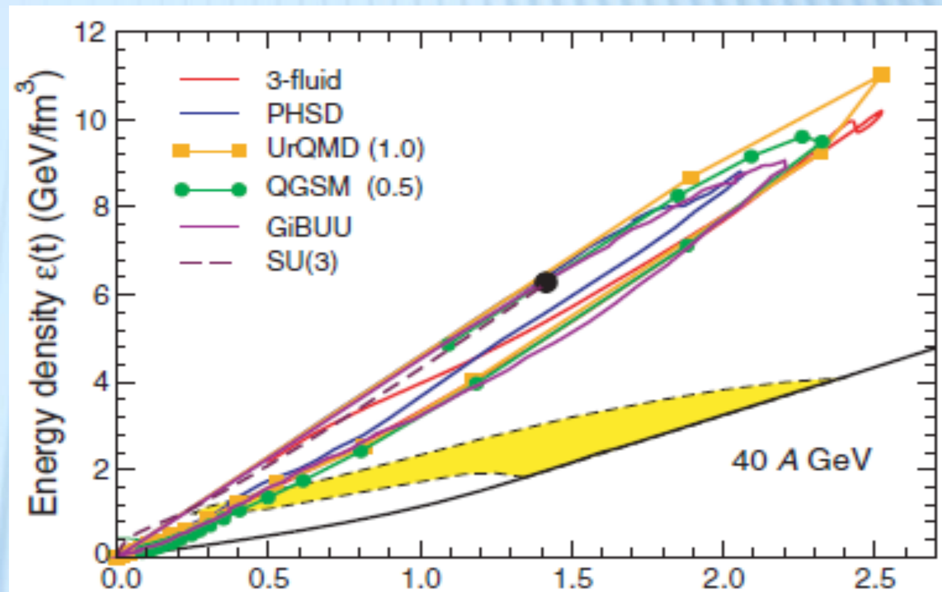

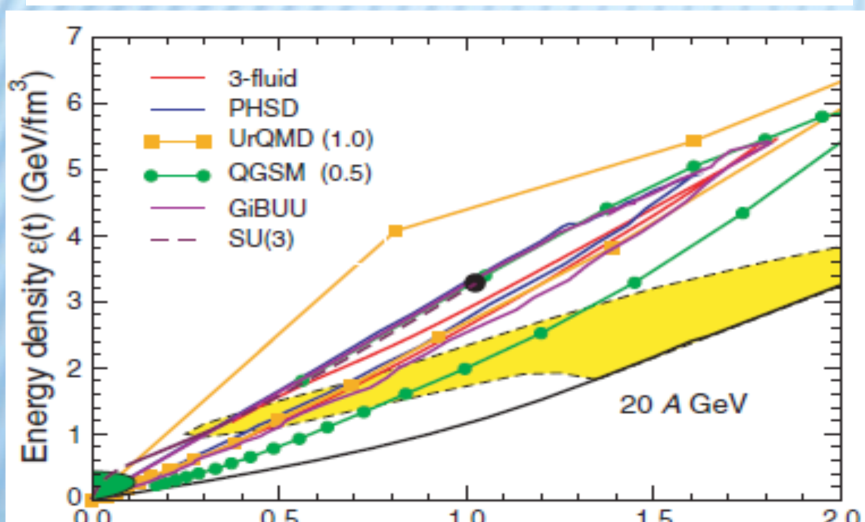

Green area : freeze-out region;
Yellow area : the phase coexistence region from schematic EOS that has a critical point at final density

Different models exhibit a large degree of mutual agreement

Infinite hadron gas: a box with periodic boundary conditions

BOX WITH PERIODIC BOUNDARY CONDITIONS

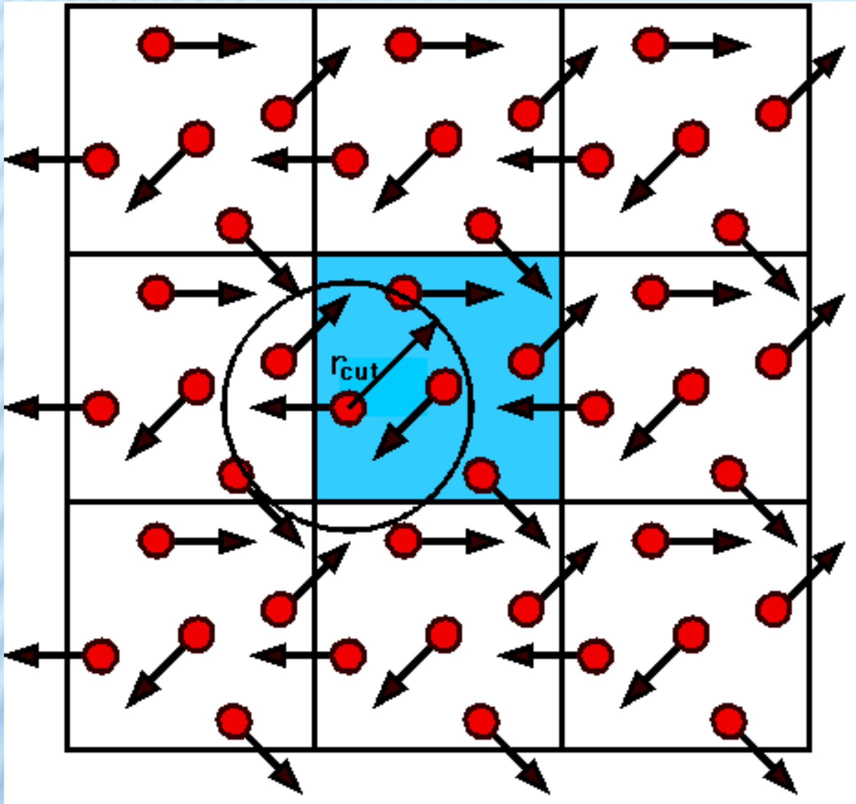

M.Belkacem et al., PRC 58, 1727 (1998)

Model employed: UrQMD
55 different baryon species (N, Δ, hyperons and their resonances with $m \leq 2.25\ \mathrm{GeV}/c^2$),
32 different meson species (including resonances with $m \leq 2\ \mathrm{GeV}/c^2$) and their respective antistates.
For higher mass excitations a string mechanism is invoked.

Initialization: (i) nucleons are uniformly distributed in a configuration space;
(ii) Their momenta are uniformly distributed in a sphere with random radius and then rescaled to the desired energy density.

Test for equilibrium: particle yields and energy spectra

BOX: PARTICLE ABUNDANCES

M.Belkacem et al., PRC 58, 1727 (1998)

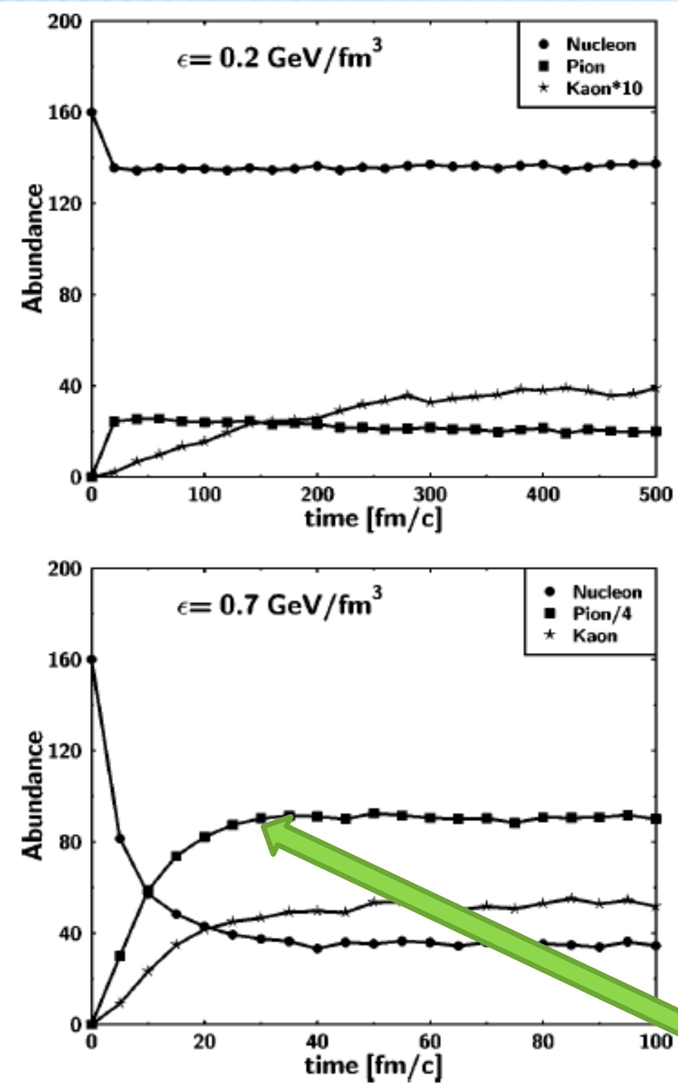

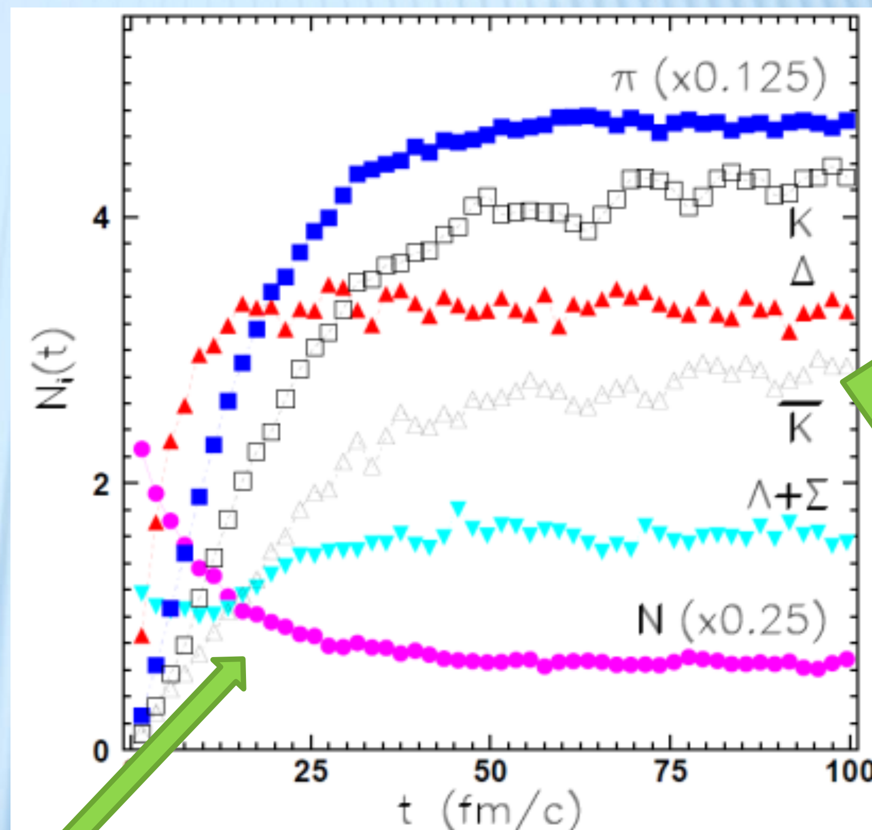

L.Bravina et al., PRC 62, 064906 (2000)

Saturation of yields after a certain time. Strange hadrons are saturated longer than others .

BOX: ENERGY SPECTRA AND MOMENTUM DISTRIBUTIONS

Fit to Boltzmann distributions ~exp(-E/T)

Fit to Gaussian distributions ~exp(-p^2/2mT)

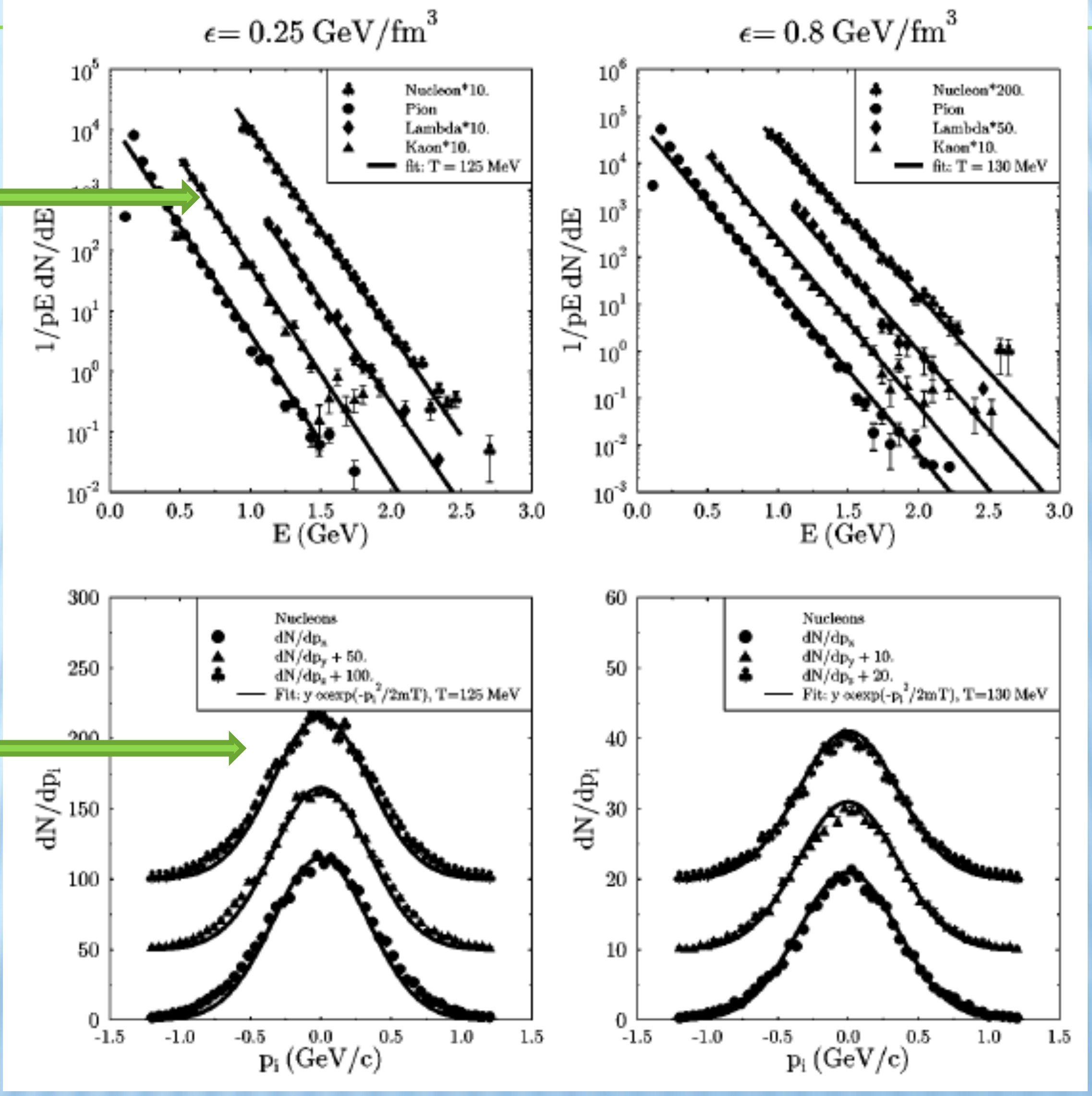

M.Belkacem et al., PRC 58, 1727 (1998)

Nearly the same temperature and complete isotropy of dN/dp_T

BOX: HAGEDORN-LIKE LIMITING TEMPERATURE

M.Belkacem et al., PRC 58, 1727 (1998)

HSD

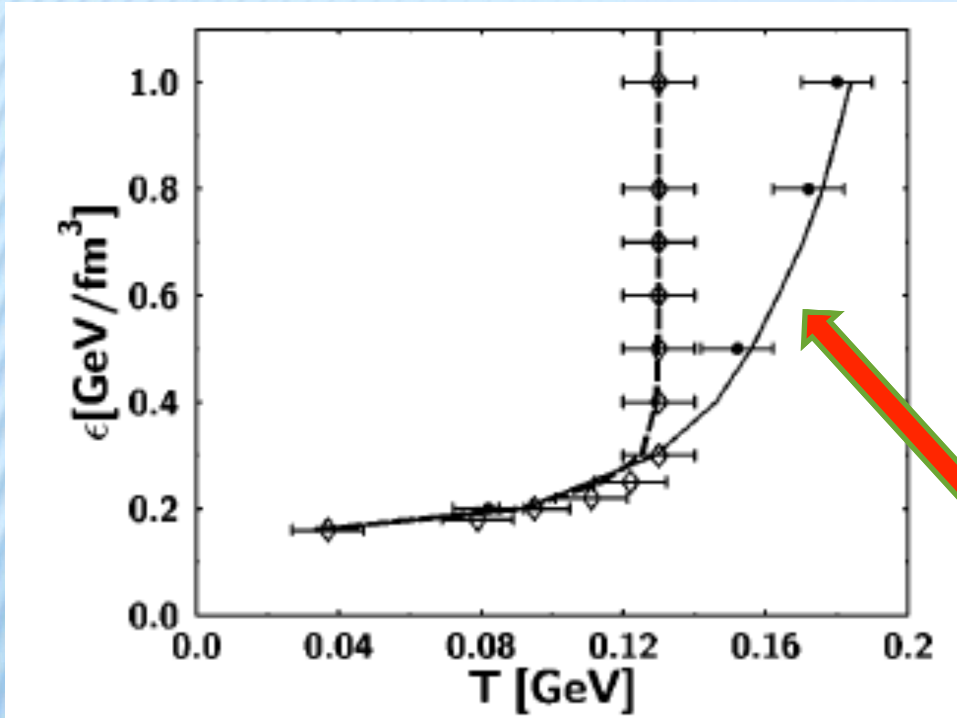

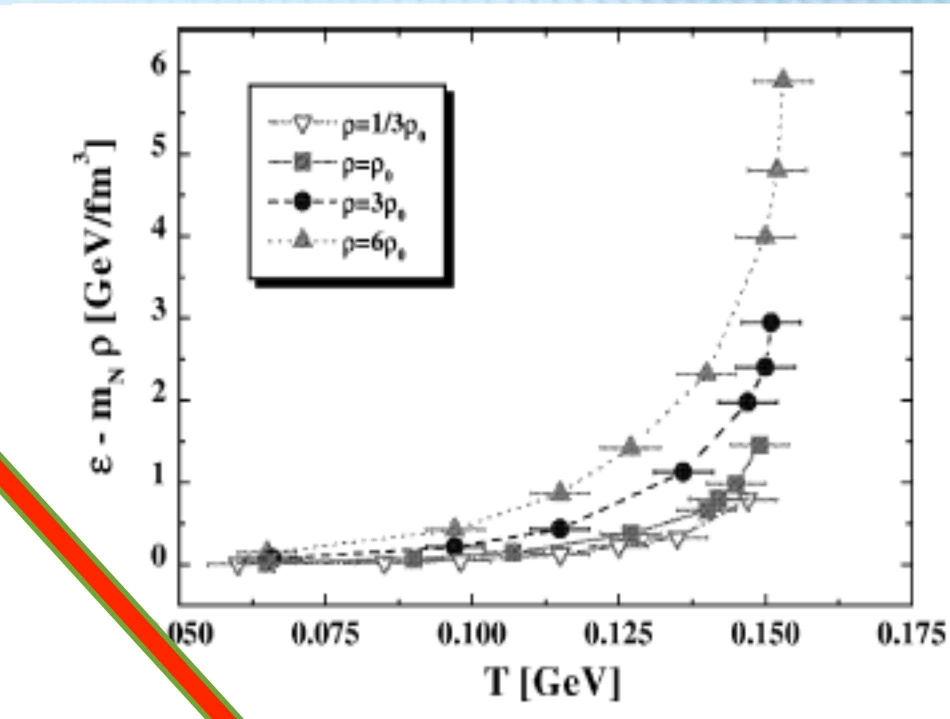

E.Bratkovskaya et al., NPA 675, 661 (2000)

UrQMD

A rapid rise of T at low ε and saturation at high energy densities. Saturation temperature depends on number of resonances in the model. W/o strings and many-N decays – no limiting T is observed.

Freeze-out of main hadron species

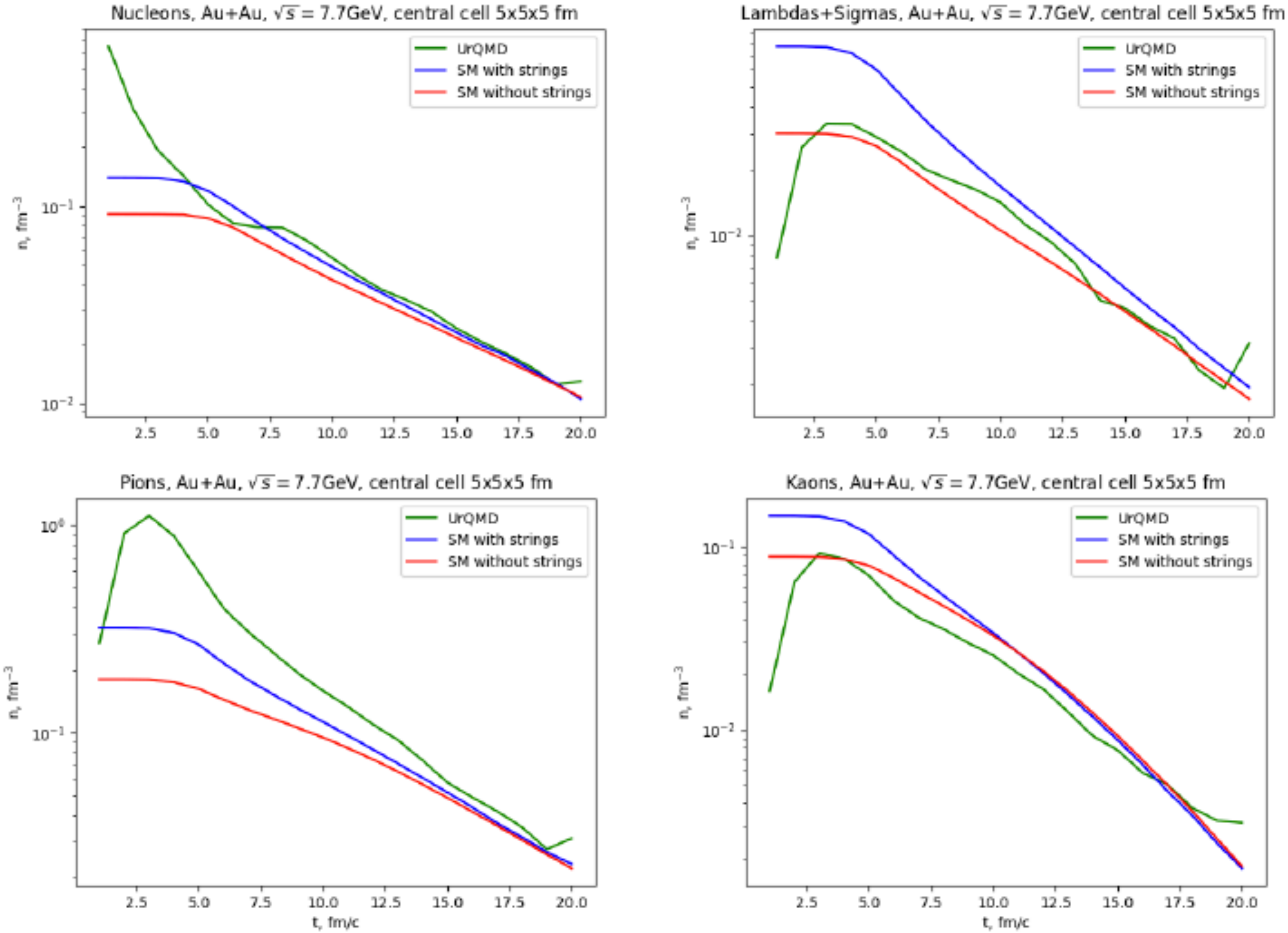

Figure 1: Particle densities in the central cell at times 1 – 20 fm/c.

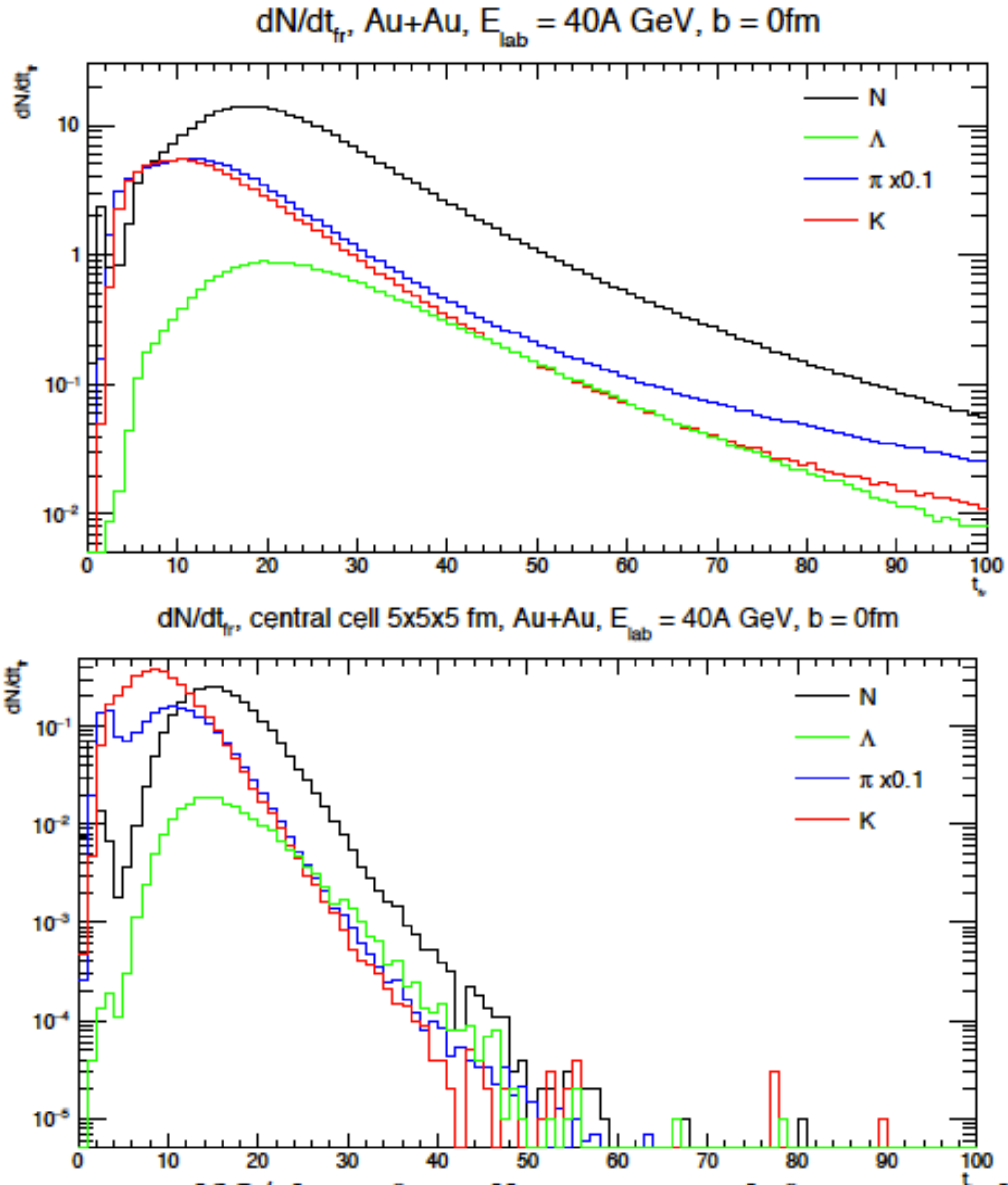

Different particles
are frozen at different space -
times
with different values of
T-μ_B-μ_S

Figure 3: dN/dt_{fr} for all space and for central cell.

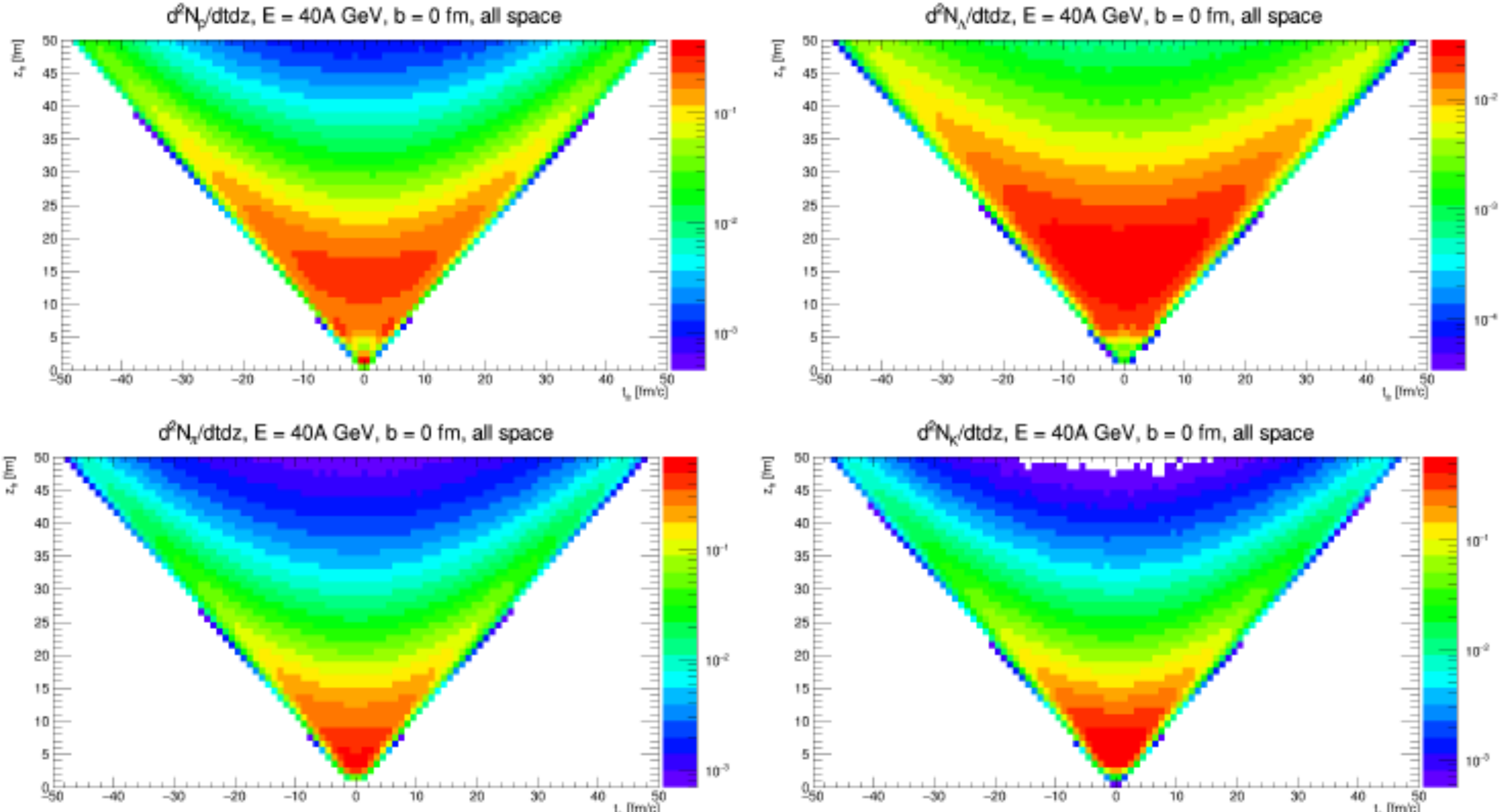

Figure 4: $d^2N/dtdz$ for protons, lambdas, pions and kaons.

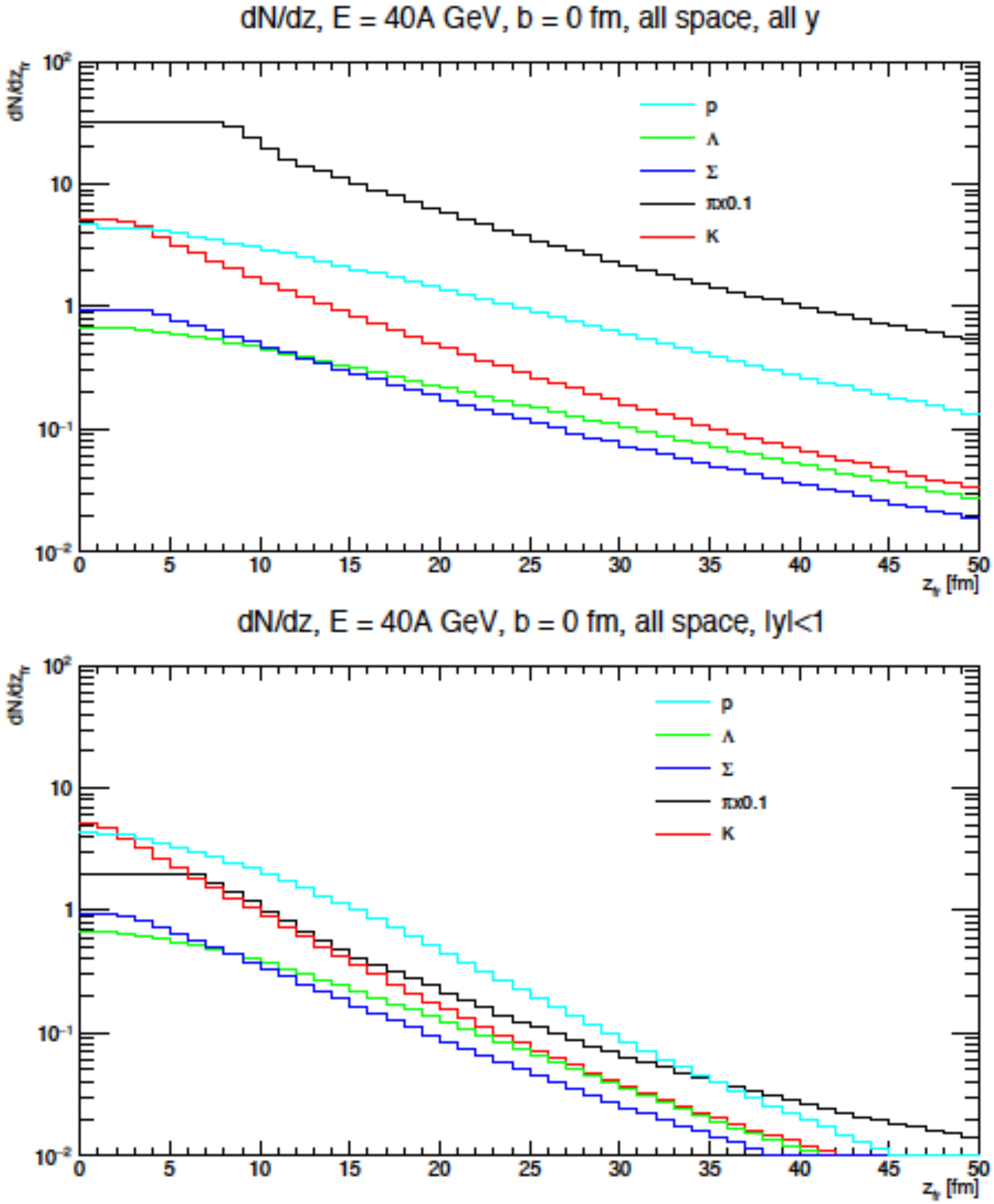

Figure 5: dN/dz for protons, lambdas, sigmas, pions and kaons for all rapidities (top figure) and for $|y| < 1$ (bottom figure). One can see that there are much more particles with large z for all rapidities, than for $|y| < 1$.

Au+Au, E_{lab}=10A GeV, b = 0 fm, all space

	All y						$\|y\| < 1$					
	t, fm/c	$\|x\|, \|y\|$, fm	$\|z\|$, fm	T, MeV	μ_b, MeV	μ_s, MeV	t, fm/c	$\|x\|, \|y\|$, fm	$\|z\|$, fm	T, MeV	μ_b, MeV	μ_s, MeV
All	18.0	4.7	6.4	112.4	473.1	72.1	18.1	4.9	5.3	110.6	492.3	70.8
p	19.7	4.7	7.2	108.6	478.1	63.0	19.6	4.9	5.7	101.9	524.5	72.5
$\overline{p}$	19.1	5.9	7.8	109.0	459.1	64.5	18.3	6.4	5.8	106.1	462.1	66.6
Λ	24.6	5.5	8.1	90.4	539.8	50.4	24.4	5.7	7.1	92.2	532.3	49.4
$\overline{\Lambda}$	23.3	6.6	8.6	98.2	487.0	58.0	22.7	6.8	7.2	96.4	497.4	54.1
Σ	20.4	4.7	6.4	105.0	496.4	56.8	20.3	4.8	5.7	101.9	524.5	72.5
$\overline{\Sigma}$	20.0	5.5	7.5	106.3	472.7	62.3	19.5	5.7	6.4	104.0	489.4	62.4
π	16.9	4.7	6.1	116.8	448.5	69.0	17.0	4.9	5.1	114.6	471.2	73.4
K	14.4	3.7	4.4	128.1	457.4	83.5	14.4	3.9	3.8	124.8	486.1	93.8
$\overline{K}$	20.9	5.3	7.1	102.9	486.2	59.9	20.8	5.5	6.1	101.0	500.6	64.8

Table 1: Average coordinates of freezeout and T, μ_b, μ_s at this coordinates.

Au+Au, E_{lab}=20A GeV, b = 0 fm, all space

	All y						$\lvert y \rvert < 1$					
	t, fm/c	$\lvert x\rvert, \lvert y\rvert$, fm	$\lvert z\rvert$, fm	T, MeV	μ_b, MeV	μ_s, MeV	t, fm/c	$\lvert x\rvert, \lvert y\rvert$, fm	$\lvert z\rvert$, fm	T, MeV	μ_b, MeV	μ_s, MeV
All	18.2	4.8	8.4	120.8	396.0	57.9	17.7	5.2	6.3	112.0	419.9	55.2
p	21.0	4.9	10.0	113.1	406.5	51.0	19.9	5.2	6.9	105.2	447.6	47.2
$\overline{p}$	20.0	6.4	9.5	110.3	390.0	51.1	18.2	7.0	6.4	110.2	406.8	52.9
Λ	26.0	5.9	11.2	93.9	481.9	34.0	25.0	6.1	8.6	90.7	488.4	48.5
$\overline{\Lambda}$	25.0	7.1	11.5	98.7	435.9	50.8	23.7	7.5	8.7	95.5	463.2	41.4
Σ	21.3	4.9	9.0	106.4	444.0	51.8	20.7	5.1	7.0	103.8	444.9	49.0
$\overline{\Sigma}$	21.1	6.2	9.4	107.1	409.4	45.5	20.1	6.6	7.3	106.0	429.6	43.1
π	16.9	4.8	7.8	121.6	394.8	66.1	16.6	5.1	6.0	115.6	397.7	55.0
K	15.1	4.0	6.3	131.8	374.8	68.0	14.8	4.2	4.9	120.6	416.2	59.6
$\overline{K}$	20.3	5.3	8.8	110.5	419.1	44.7	19.7	5.6	6.8	105.2	447.6	47.2

Table 2: Average coordinates of freezeout and T, μ_b, μ_s at this coordinates.

Au+Au, E_{lab}=30A GeV, b = 0 fm, all space

	All y						$\|y\| < 1$					
	t, fm/c	$\|x\|,\|y\|$, fm	$\|z\|$, fm	T, MeV	μ_b, MeV	μ_s, MeV	t, fm/c	$\|x\|,\|y\|$, fm	$\|z\|$, fm	T, MeV	μ_b, MeV	μ_s, MeV
All	18.6	5.0	9.7	120.1	370.0	42.9	17.6	5.3	6.8	113.2	393.4	47.9
p	22.3	5.1	12.0	115.5	355.4	35.5	20.3	5.4	7.5	108.8	404.4	52.3
$\overline{p}$	20.7	6.6	10.7	111.4	373.6	38.0	18.4	7.2	6.7	107.9	363.1	33.8
Λ	27.2	6.0	13.3	97.4	428.9	39.1	25.5	6.3	9.4	93.2	464.7	39.7
$\overline{\Lambda}$	26.1	7.3	12.9	97.9	420.0	35.7	24.1	7.8	9.1	96.9	431.4	34.6
Σ	22.3	5.1	10.7	109.4	392.4	37.1	21.2	5.3	7.7	104.0	427.5	45.3
$\overline{\Sigma}$	22.0	6.4	10.9	107.0	397.3	36.7	20.3	6.8	7.6	107.6	399.5	37.5
π	17.4	4.9	9.0	126.9	343.5	42.2	16.6	5.3	6.6	116.3	375.0	43.1
K	15.9	4.1	7.6	127.2	344.8	46.4	15.2	4.4	5.5	124.9	362.4	56.3
$\overline{K}$	20.5	5.3	9.8	114.4	380.6	50.1	19.3	5.6	7.2	112.1	393.3	49.7

Table 3: Average coordinates of freezeout and T, μ_b, μ_s at this coordinates.

Au+Au, E$_{lab}$=40A GeV, b = 0 fm, all space

	All y						$\|y\| < 1$					
	t, fm/c	$\|x\|, \|y\|$, fm	$\|z\|$, fm	T, MeV	μ_b, MeV	μ_s, MeV	t, fm/c	$\|x\|, \|y\|$, fm	$\|z\|$, fm	T, MeV	μ_b, MeV	μ_s, MeV
All	19.1	5.0	10.6	122.7	321.6	41.3	17.7	5.4	7.2	116.5	358.8	41.6
p	23.4	5.2	13.6	115.8	343.2	37.8	20.7	5.5	7.9	105.2	403.5	37.8
$\overline{p}$	21.5	6.7	11.5	114.9	340.4	32.7	18.8	7.2	7.0	109.0	351.8	33.6
Λ	28.3	6.2	14.9	96.2	423.3	20.2	25.9	6.5	10.0	91.0	459.3	33.3
$\overline{\Lambda}$	27.0	7.4	14.0	96.8	413.7	30.7	24.5	7.9	9.4	95.4	423.0	31.8
Σ	23.1	5.2	12.0	107.8	391.3	25.4	21.6	5.5	8.2	102.9	416.3	37.2
$\overline{\Sigma}$	22.7	6.4	11.8	107.8	380.0	28.7	20.7	6.9	7.9	103.6	402.3	42.6
π	17.8	5.0	9.8	125.6	323.4	39.1	16.7	5.4	6.9	117.5	359.8	40.5
K	16.6	4.3	8.6	126.3	332.3	42.1	15.5	4.5	5.9	120.2	371.5	52.8
$\overline{K}$	20.7	5.4	10.6	113.6	359.6	30.6	19.3	5.7	7.5	111.9	379.5	34.9

Table 4: Average coordinates of freezeout and T, μ_b, μ_s at this coordinates.

Consequences of the different space-time freeze-out:

- Differences in yields in SM

The difference between average freeze-out and freeze-out for particular species is very large

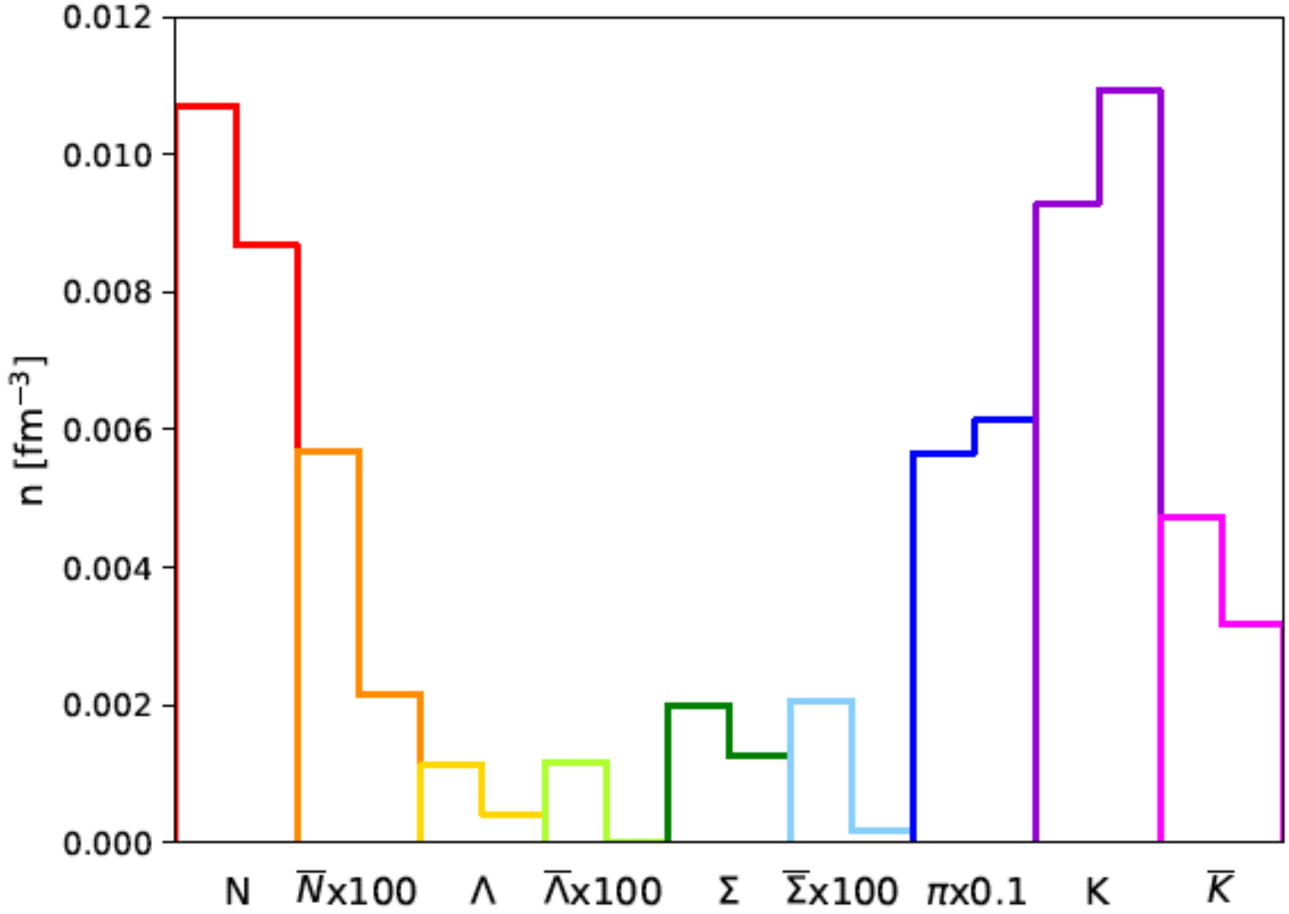

Figure 4: Particle densities at average freezeout coordinates of all particles (left column) and at freezeout coordinates of each particle type (right column) from statmodel; at average freezeout coordinates of all particles (star) and at freezeout coordinates of each particle type (pentagon) from UrQMD. E = 40*A* GeV.

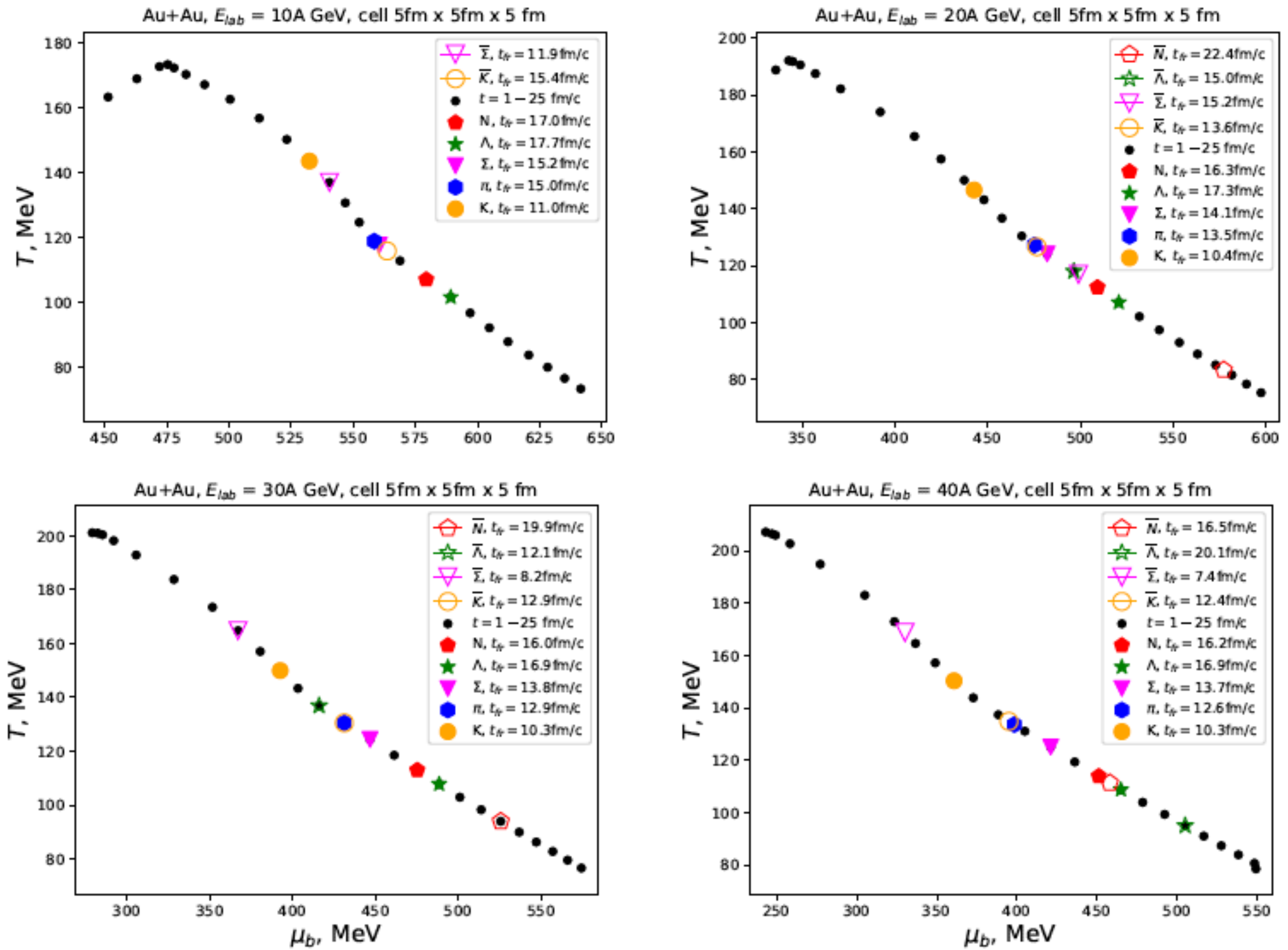

Figure 2: $T(\mu_B)$ in the central cell. Average freezeout times of different particles in the central cell are marked by colored markers.

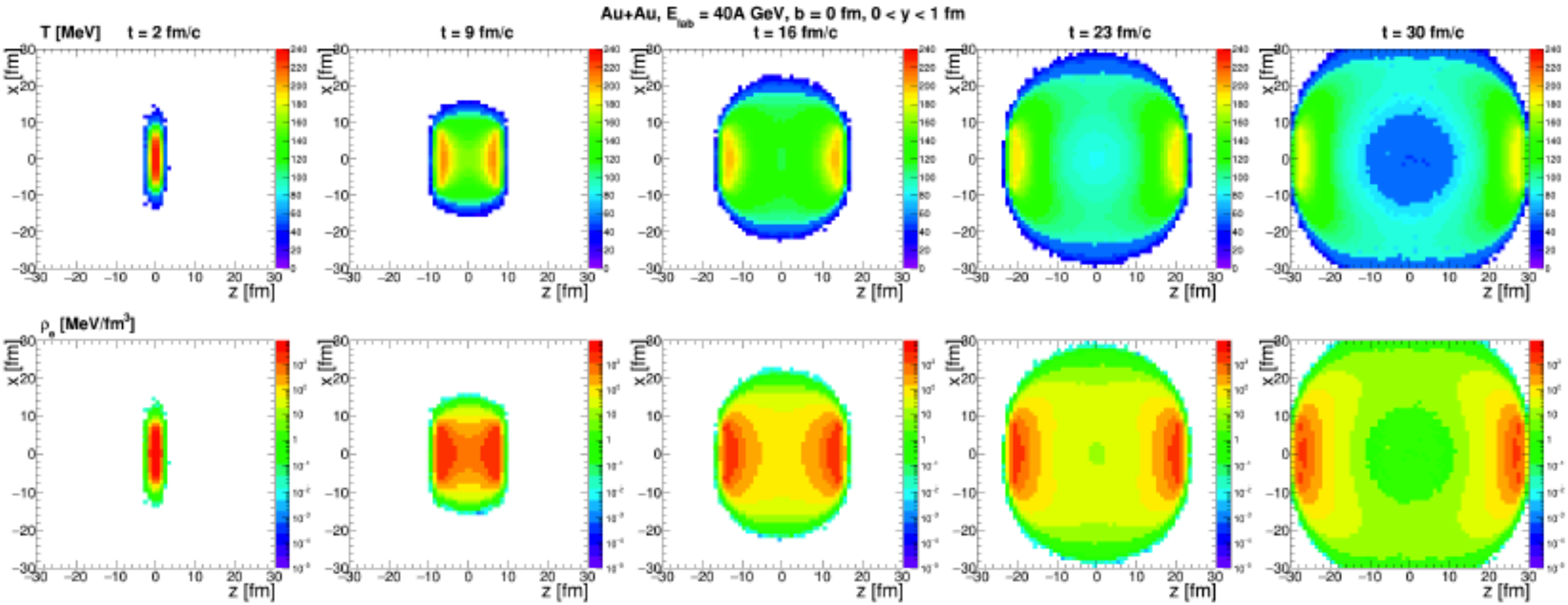

Figure 5: T and ε spatial distributions.

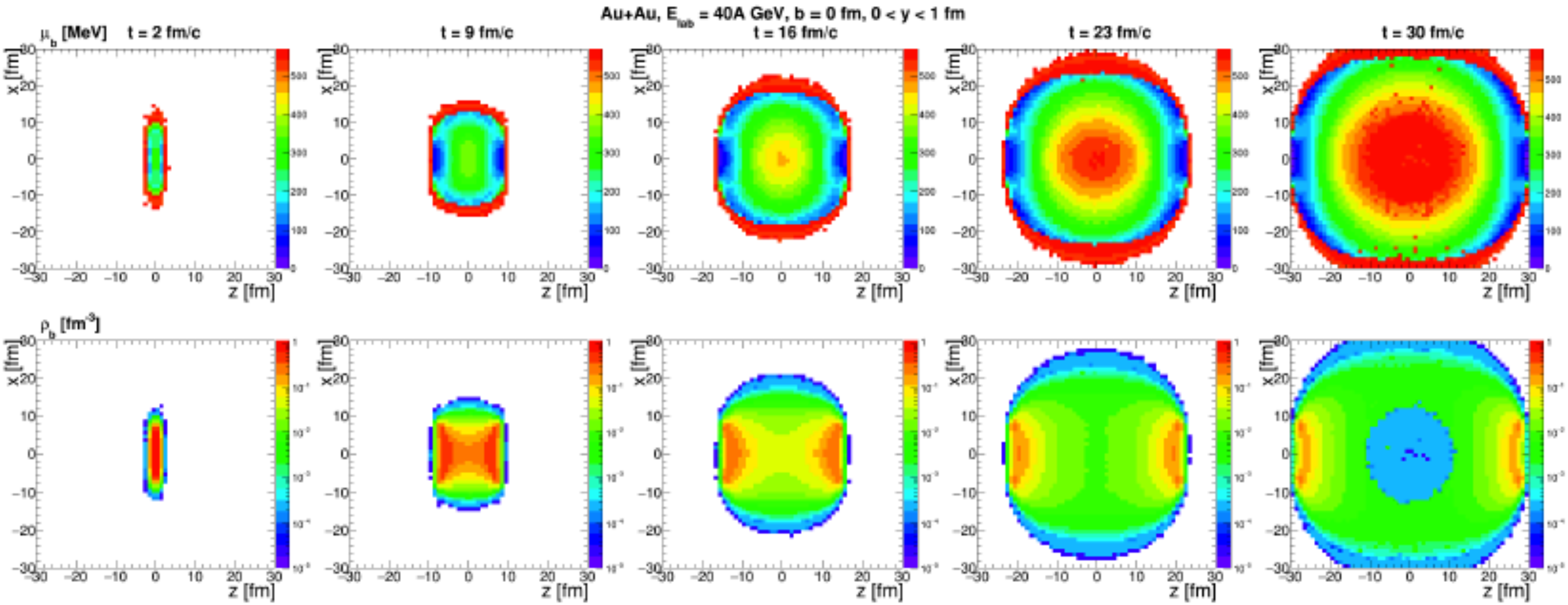

Figure 6: μ_b and ρ_b spatial distributions.

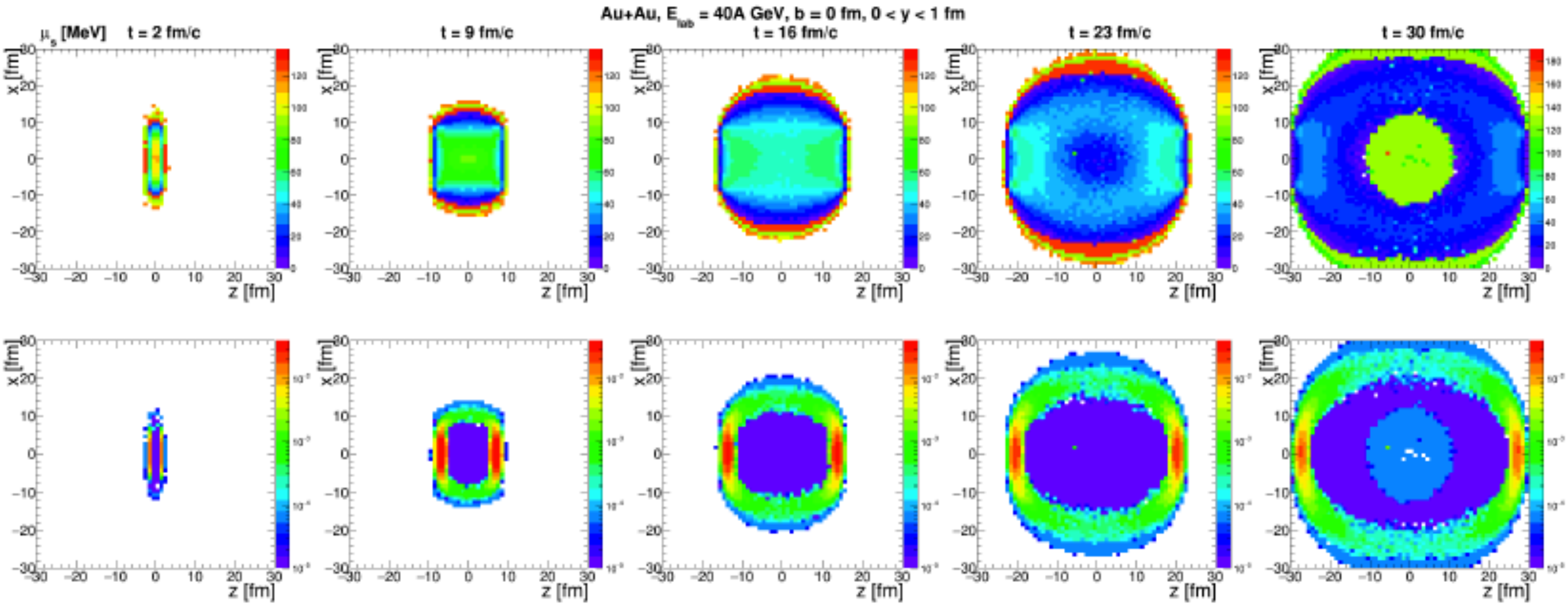

Figure 7: μ_s and ρ_s spatial distributions.

Conequences of the different space-time freeze-out:

- Directed flow

Space distribution of Lambdas

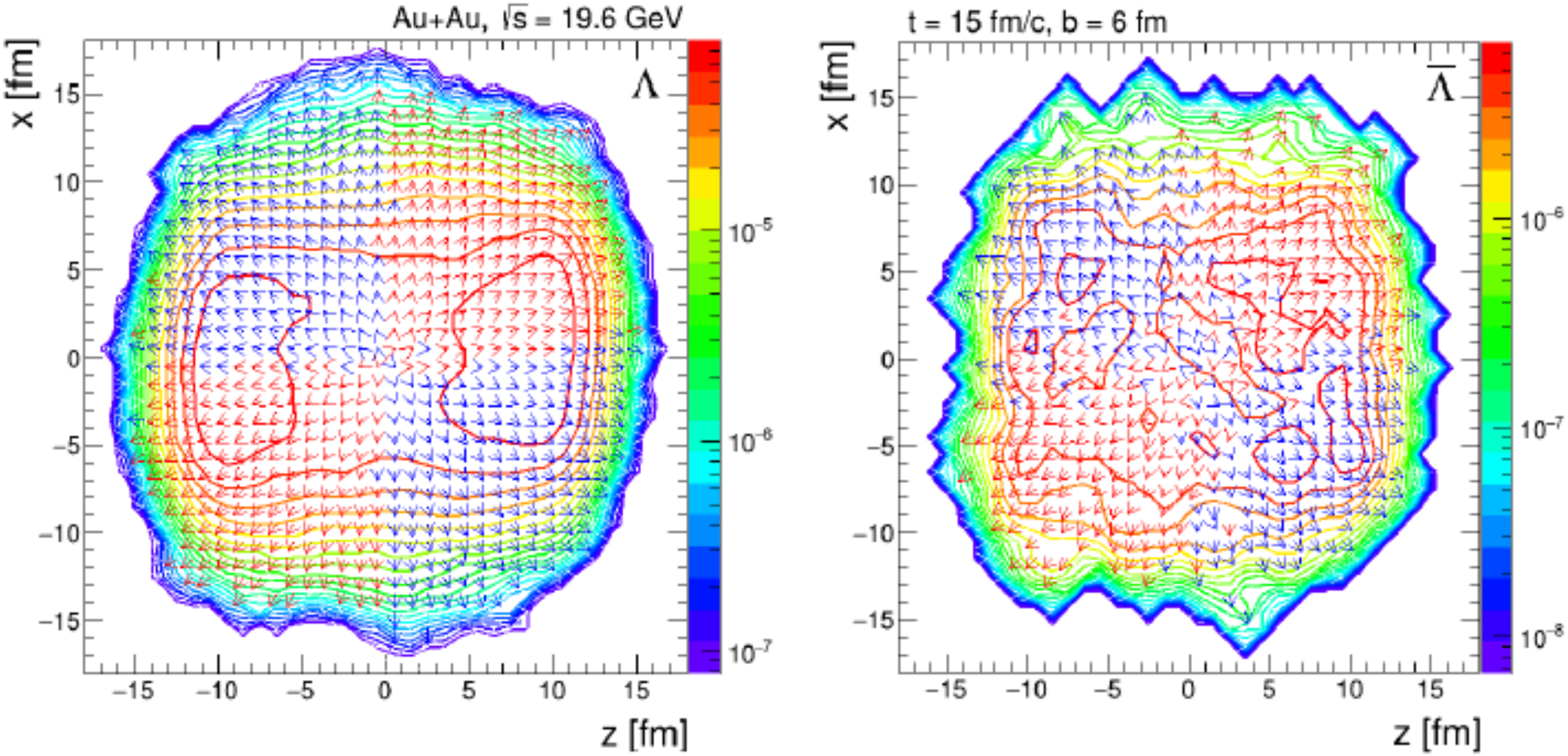

At $\sqrt{s} = 19.6 GeV$ Λ are mostly located near hot and dense regions and $\bar{\Lambda}$ are distributed more uniformly near system center.

Space distribution of Lambdas

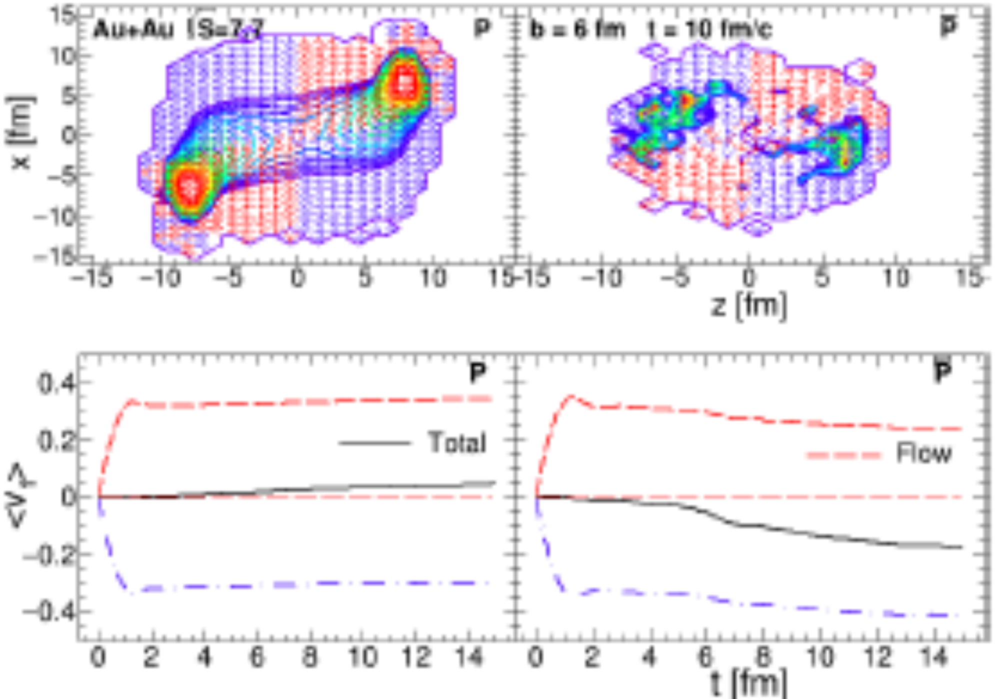

At low energies Λ and $\bar{\Lambda}$ are produced and emitted from the same regions as protons and antiprotons respectively. Λ's are concentrated also near hot and dense spectators, whereas $\bar{\Lambda}$'s are mostly produced in central region.

Mean flow is calculated as:

$$< v_1 >= \int sign(y) v_1(y) \frac{dN^{par}}{dy} dy / \int \frac{dN^{par}}{dy} dy$$

Collective velocities are shown on the picture to demonstrate that particles which have positive product of velocities $v_x v_z$ produce normal component of flow and particles with $v_x v_z < 0$ produce anti-flow component of directed flow. [Bravina et al, EPJ Web of Conferences 191, 05004 (2018)]

Directed flow for Lambdas and kaons

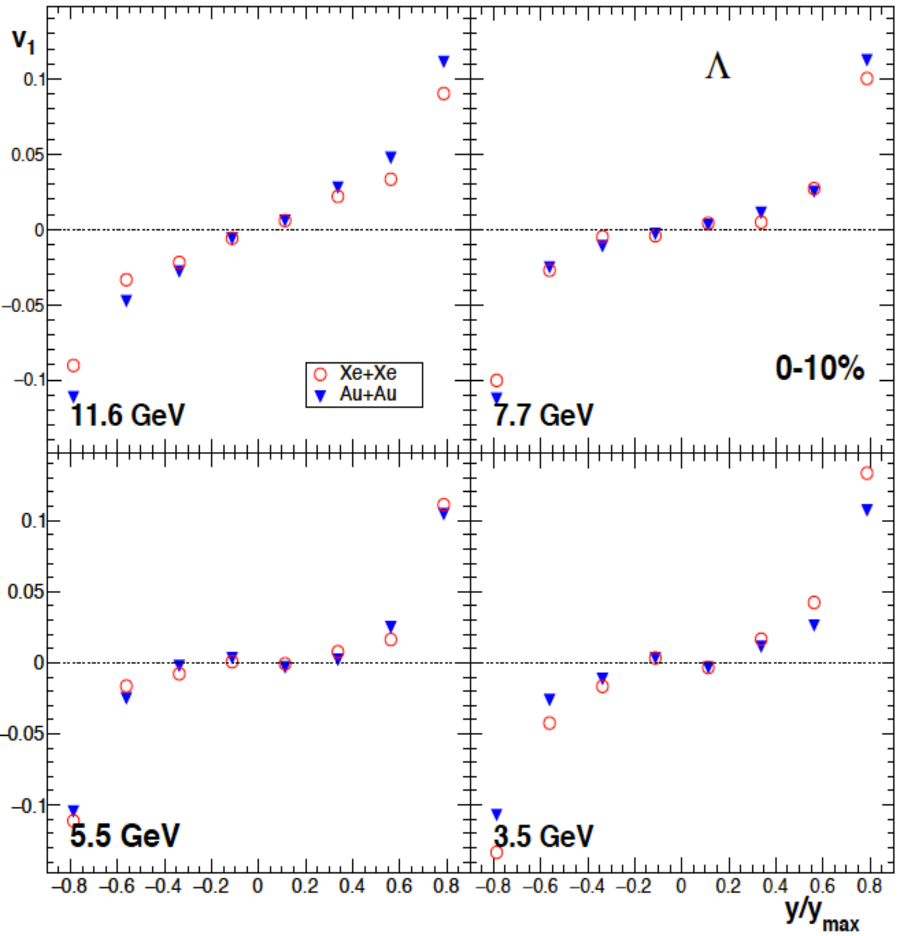

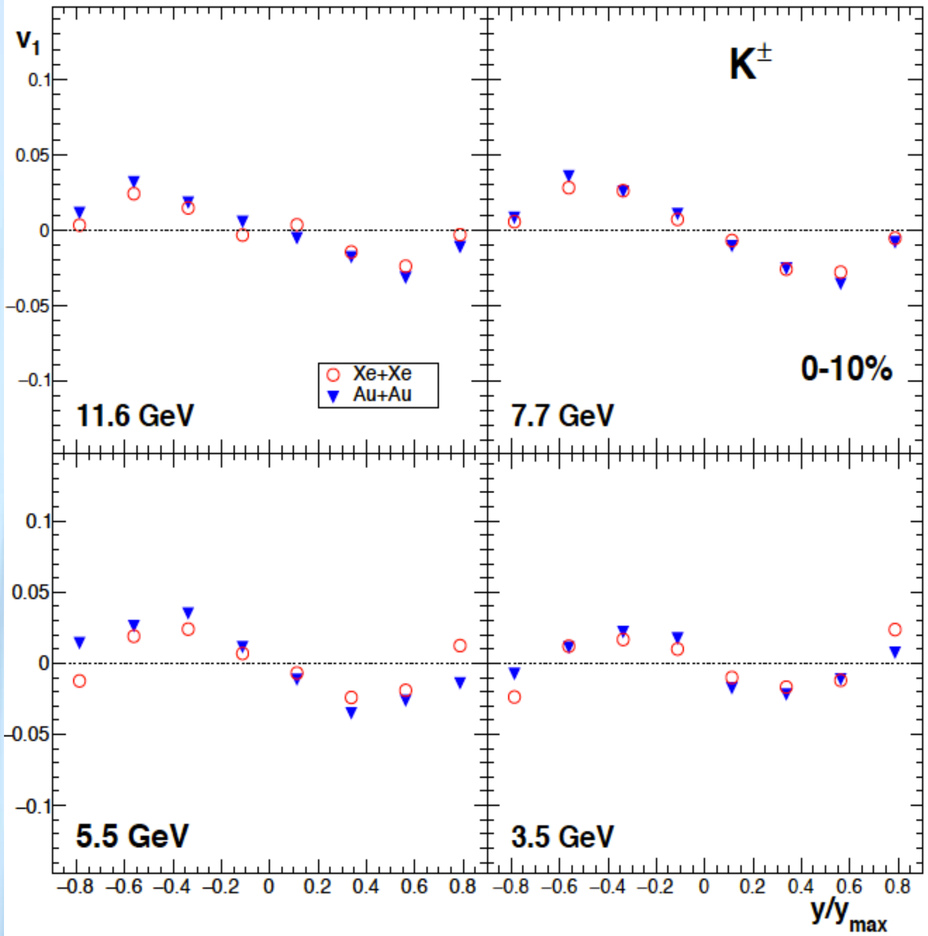

V_1 for Λ changes sign at midrapidity with decreasing collision energy, whereas V_1 for kaons has negative slope (antiflow)

Different slopes of different particles: URQMD and Data

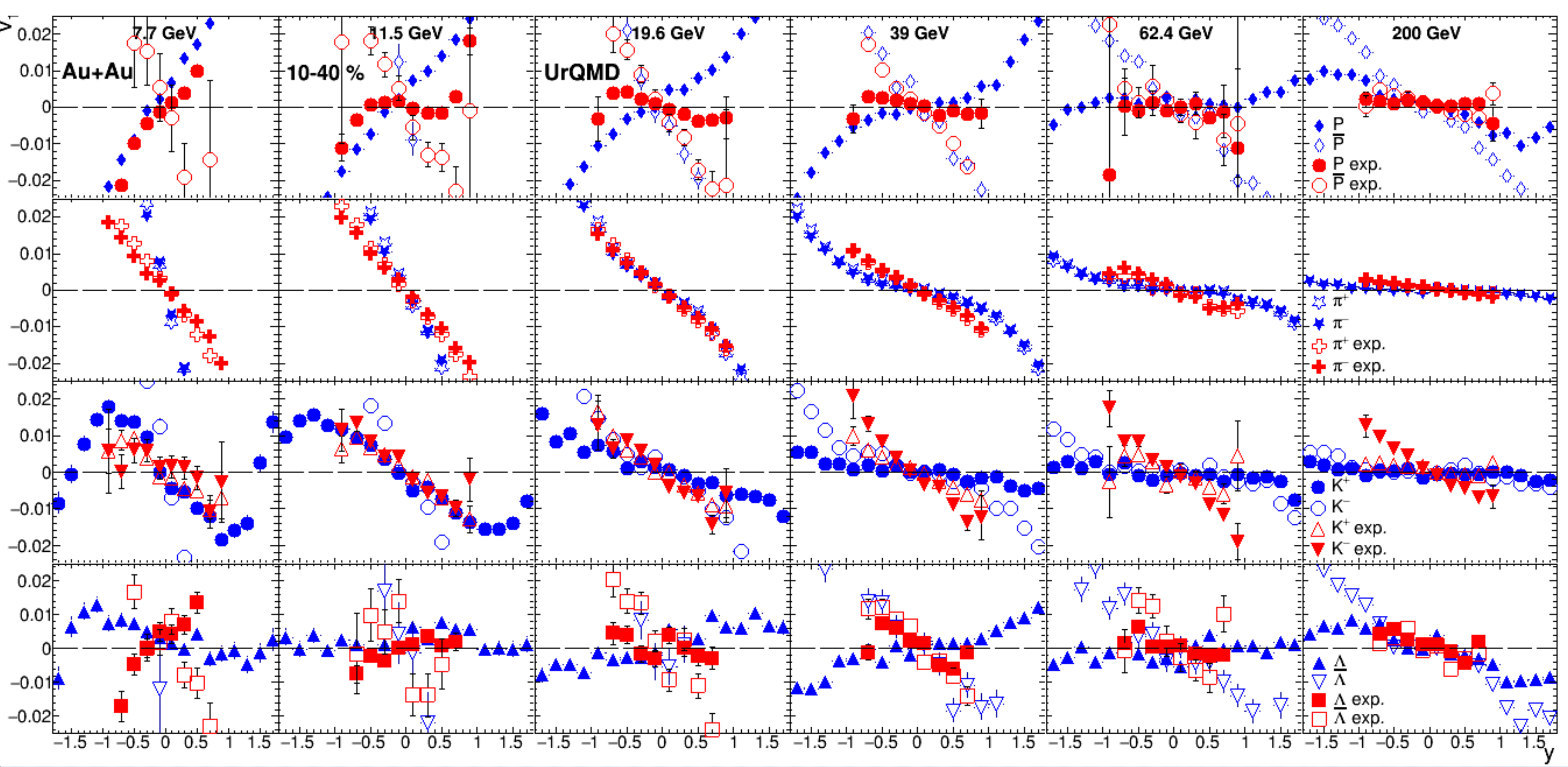

Consequences of the different space-time freeze-out:

- Difference in **Polarization** for lambdas and antilambdas

Polarization energy dependency

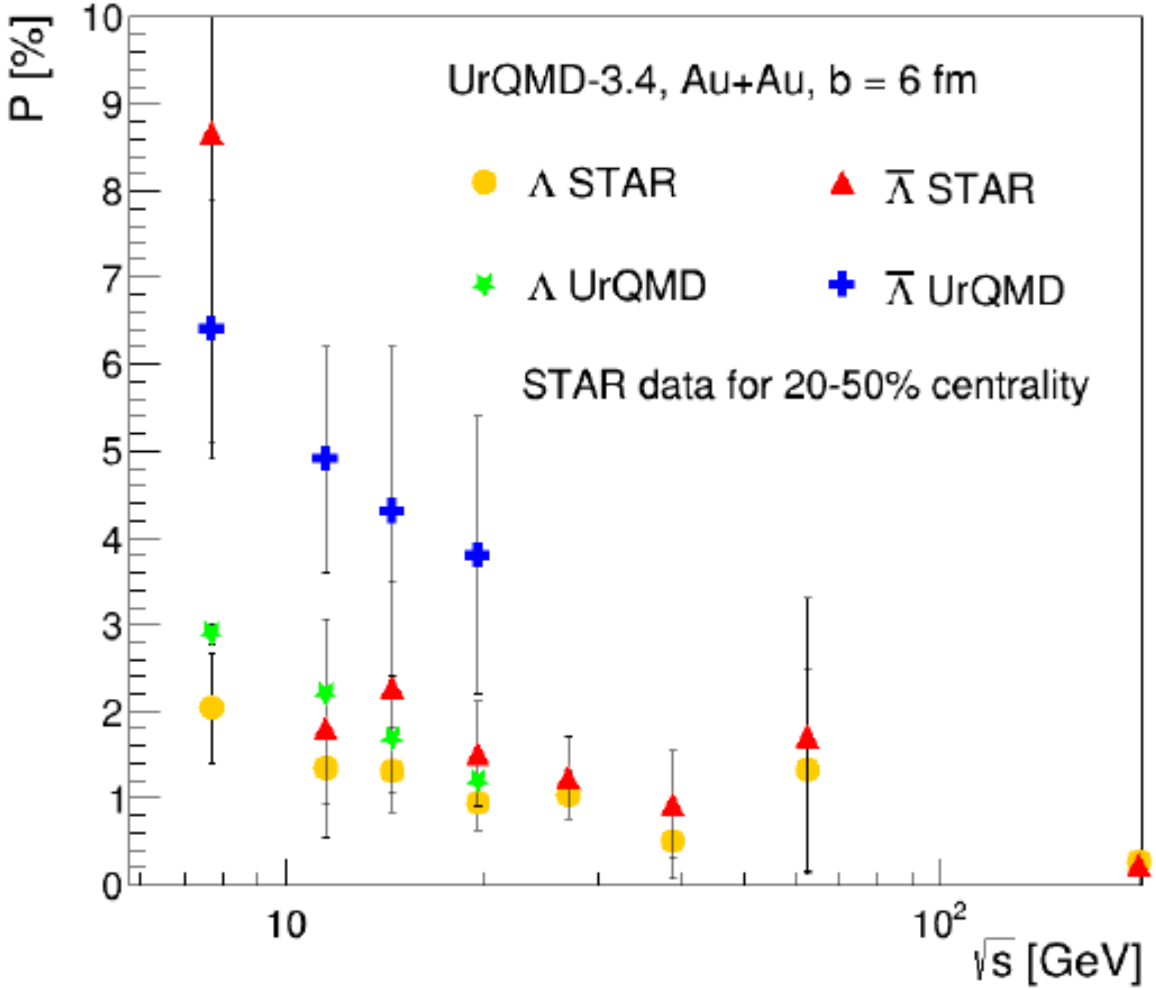

Polarization of Λ and $\bar{\Lambda}$ decreases with energy as in the experiment.
Λ's global polarization agrees well with experimental data. $\bar{\Lambda}$ polarization has right energy dependence.

STAR data from [Phys. Rev. C 98 (2018) 14910]

Freeze-out

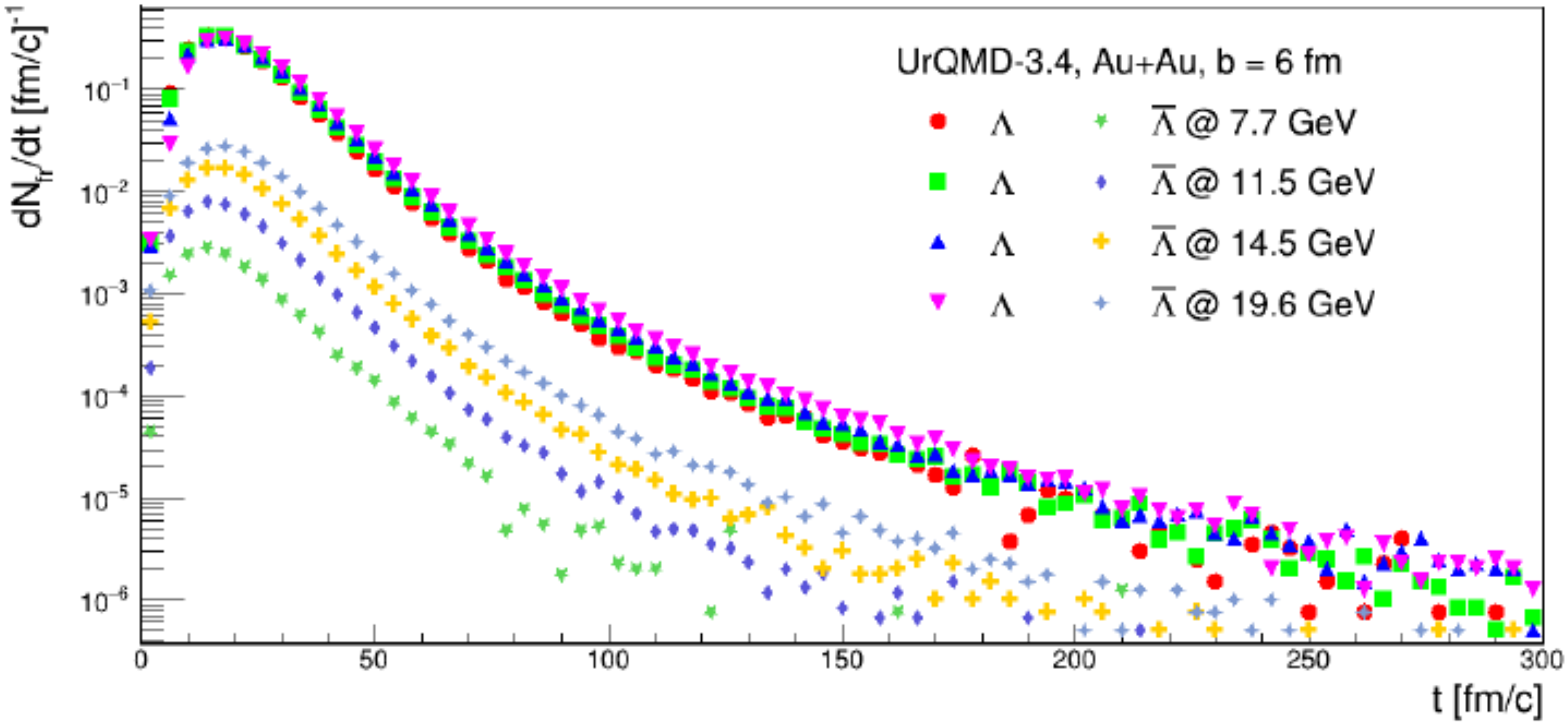

Λ's and $\bar{\Lambda}$'s with $|y| < 1$ and $0.2 < p_t < 3$ GeV/c were analyzed.

$\sqrt{s}$ [GeV]	7.7	11.5	14.5	19.6
Mean freeze-out time Λ [fm/c]	21.3009	21.9568	23.066	24.3462
Mean freeze-out time $\bar{\Lambda}$ [fm/c]	19.7806	21.0302	21.959	23.1288

Proper Temperature

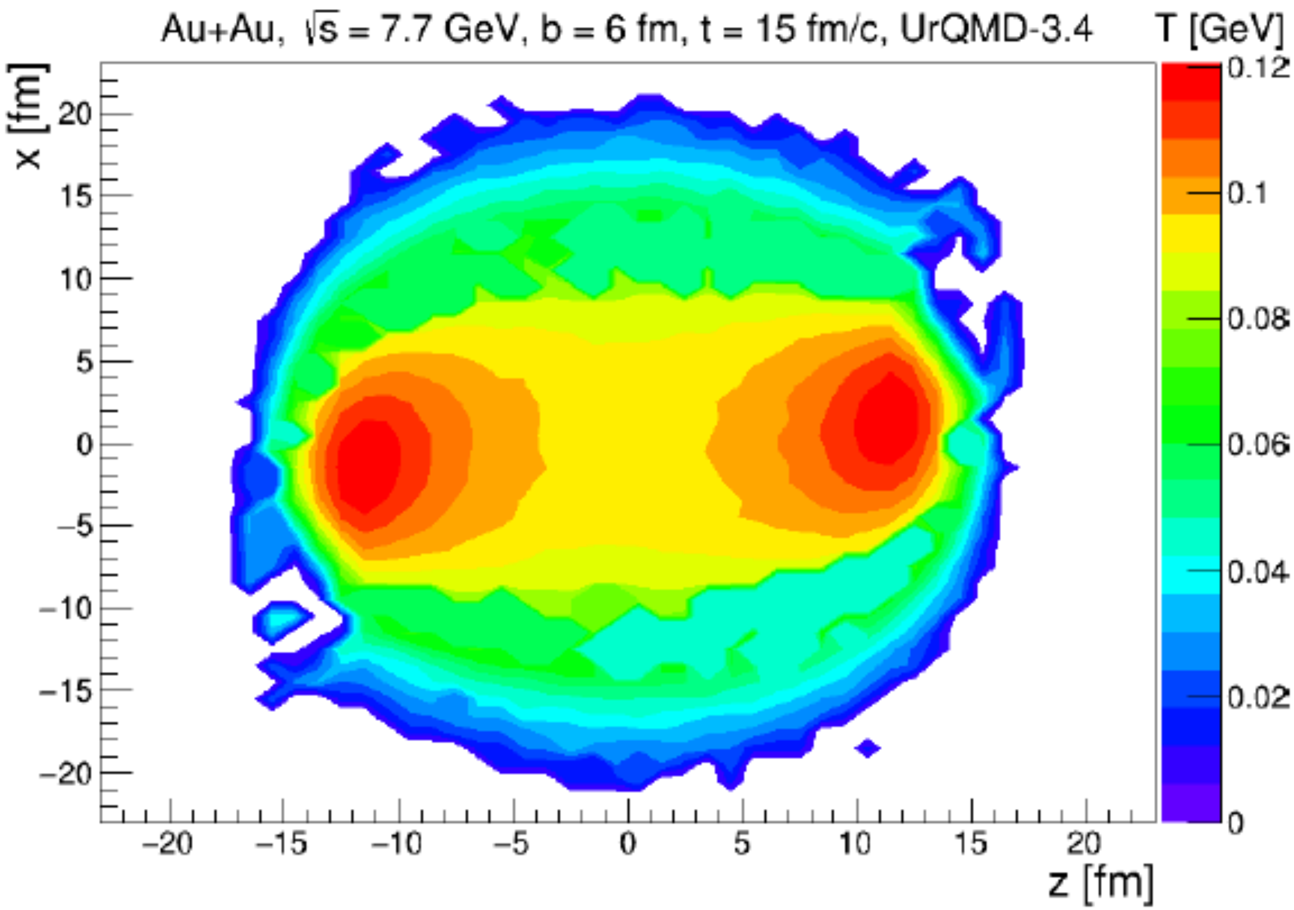

Temperature extracted with statistical model is not uniform. There are two main regions. More hot regions with T $\simeq 100 MeV$ are connected to dense spectators. The other part is related to fireball with temperature $\simeq 60 MeV$.

Thermal vorticity in reaction plane

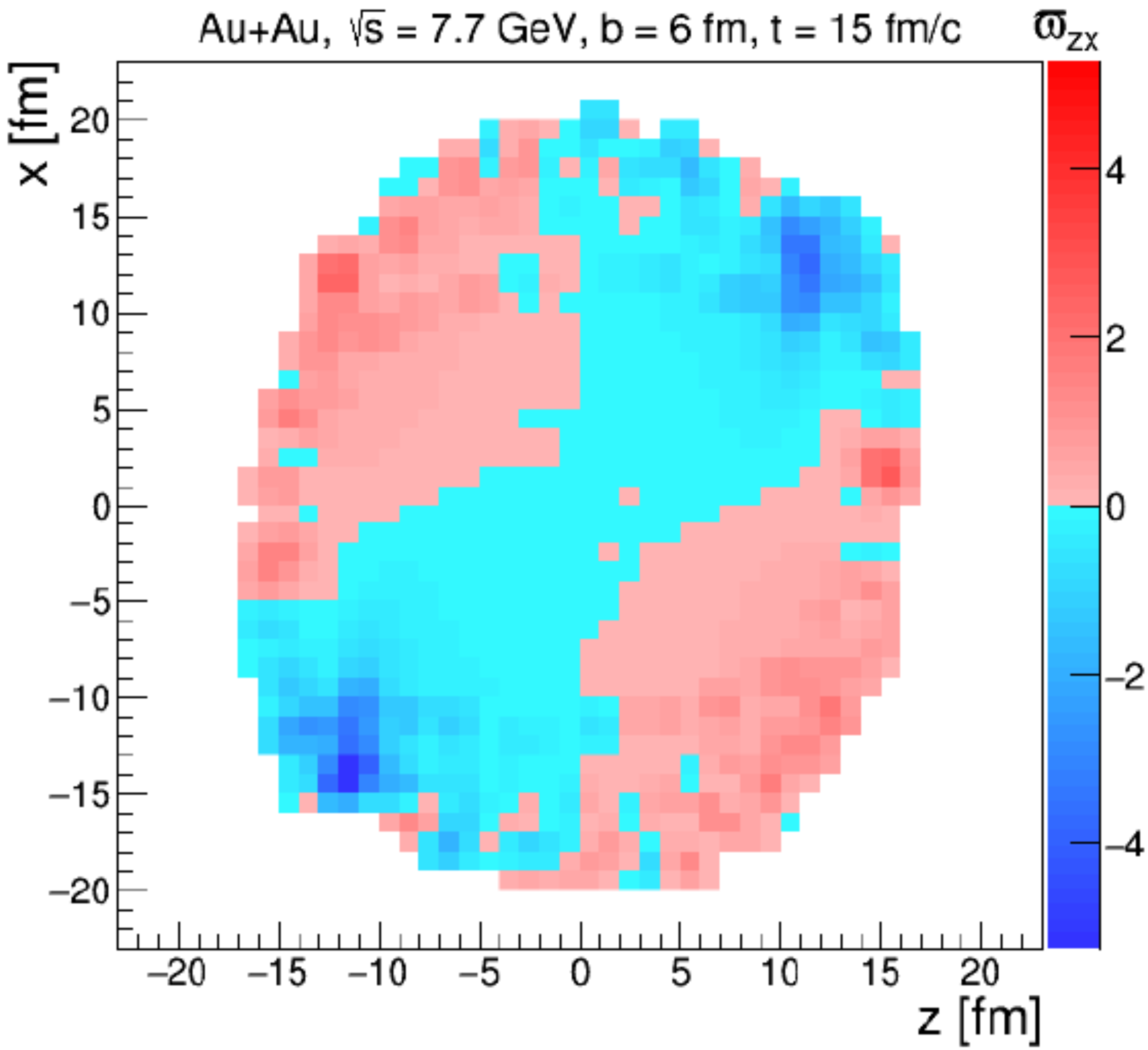

Thermal vorticity component ϖ_{zx} has quadruple-like structure in reaction plane which is stable in time but magnitude decreases due to system expansion. First and third quadrant are connected with central region which has small negative vorticity. This connection part becomes smaller when energy increases.

Emission of Λ and $\bar{\Lambda}$

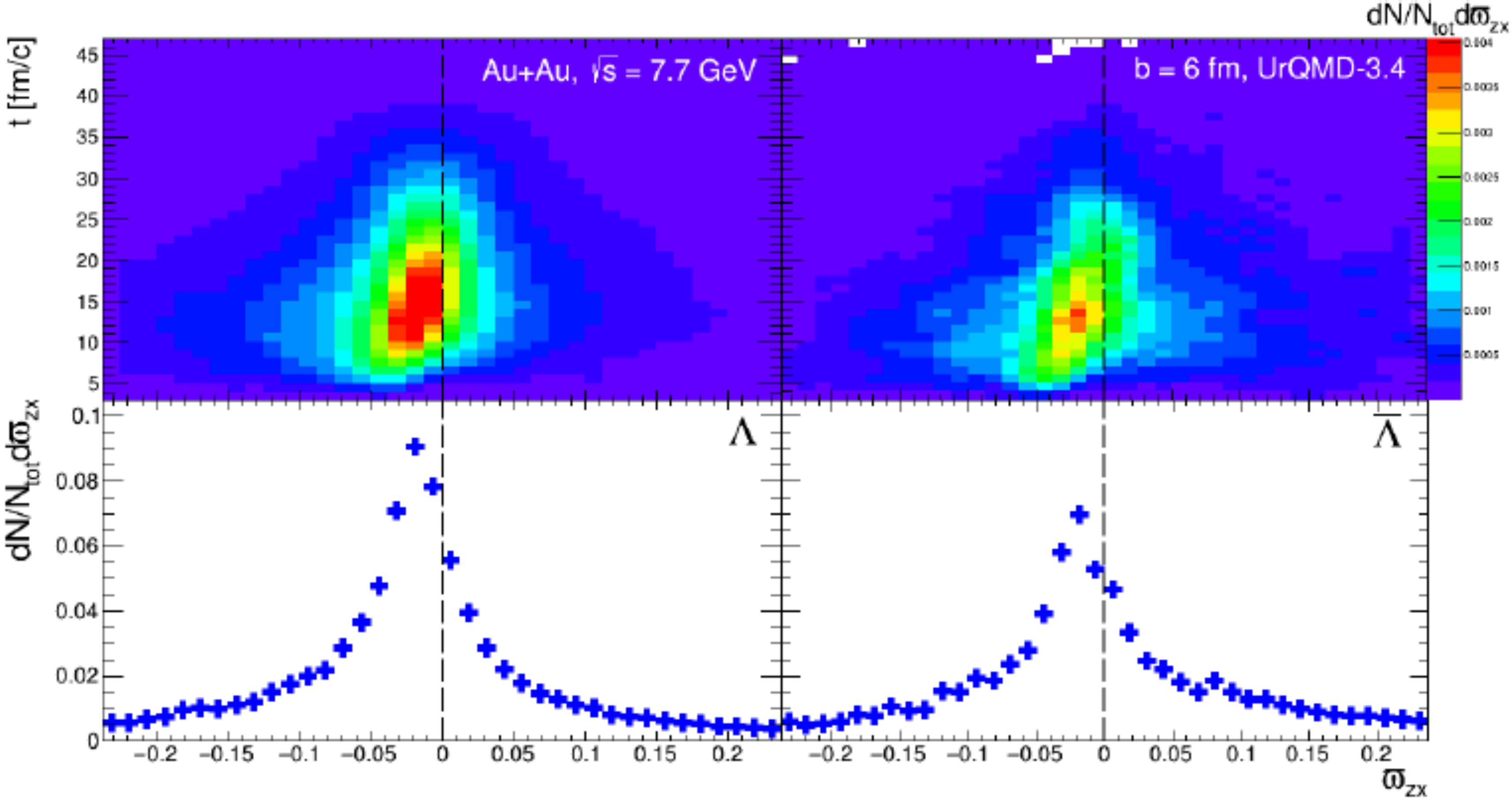

At $\sqrt{s} = 7.7 GeV$ Λ and $\bar{\Lambda}$ are mainly emitted from regions with small negative vorticity, thus they should have non-zero positive polarization. $\bar{\Lambda}$ has mean value of ϖ_{zx} with larger magnitude than Λ ($\simeq -0.04$ and $\simeq -0.017$ respectively).

Emission of Λ and $\bar{\Lambda}$

At $\sqrt{s} = 19.6 GeV$ Λ and $\bar{\Lambda}$ are also mainly emitted from regions with small negative vorticity, but distributions are more symmetric and wide. Thus mean values of ϖ_{zx} for Λ and $\bar{\Lambda}$ drop ($\simeq -0.009$ and $\simeq -0.011$ respectively).

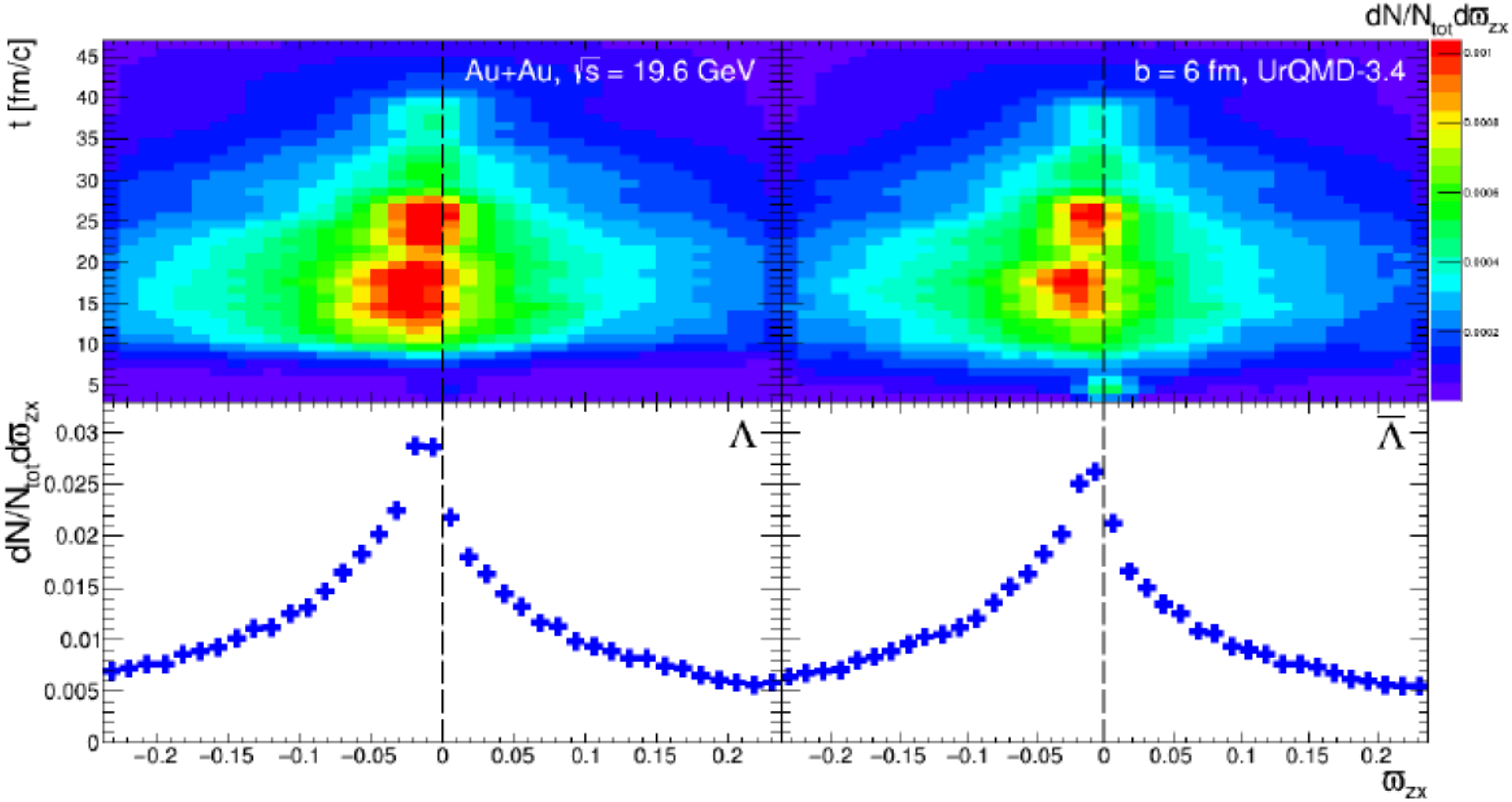

Polarization time evolution

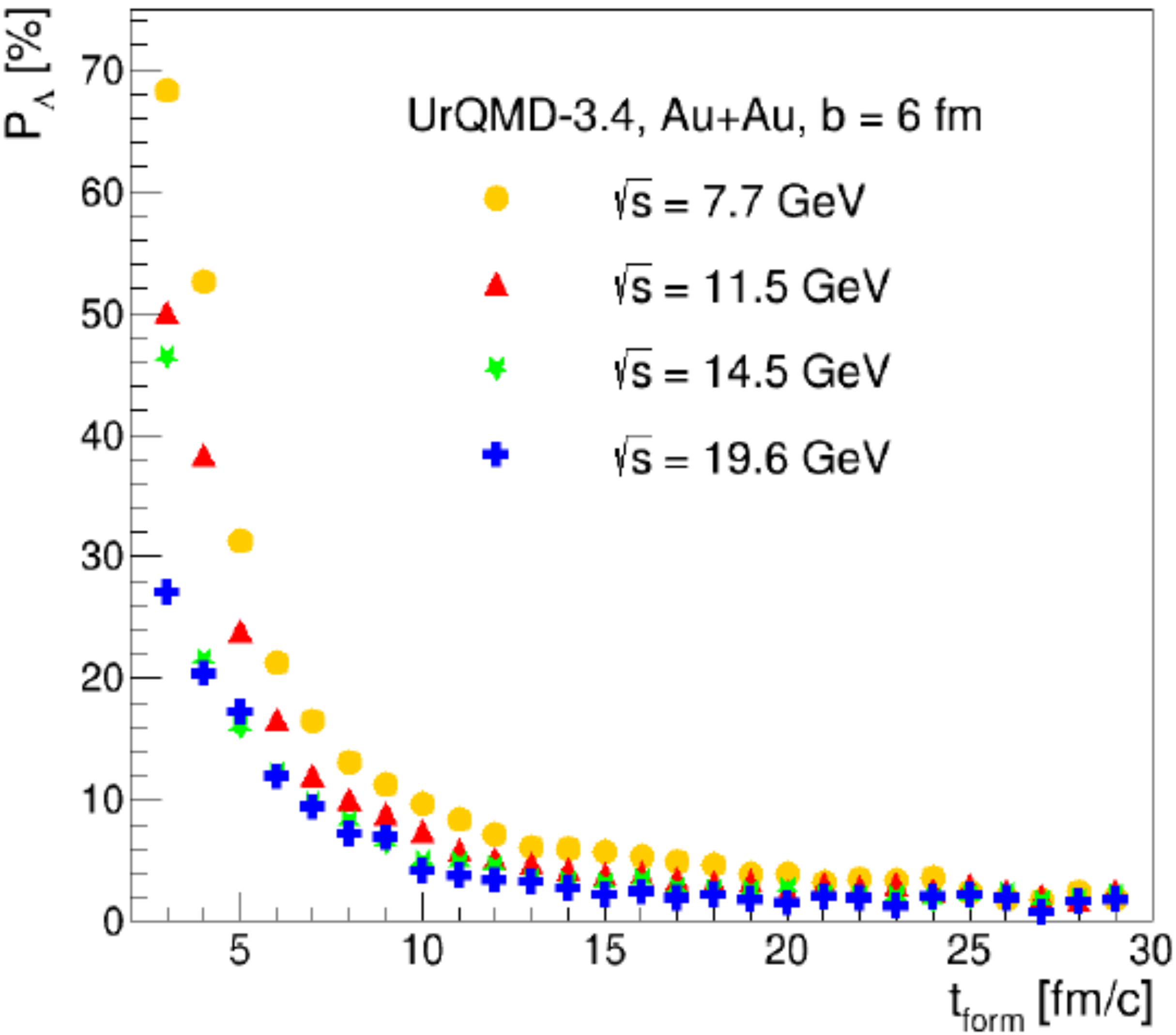

Polarization of Λ hyperon decreases with time. At the beginning lambdas are preferably formed in hot and dense regions with high polarization. But later lambdas are formed uniformly in fireball and average polarization is almost zero.

Conclusions

- ***MC models favor chemical equilibration of hot and dense nuclear matter at $t \approx 7$ fm/c***
- ***The EOS has a simple form: $P/\varepsilon = const$ (hydro!) even at far-from-equilibrium stage. The speed of sound C^2_s varies from 0.12 (AGS) to 0.14 (40 AGeV), and to 0.15 (SPS & RHIC) => saturation***
- ***In MC models different particles are frozen at different times: K-π-antiΣ-Σ,antip-p-antiΛ-Λ***

and in different space regions with different **T-μ_B-μ_S**

It naturally explanes such effects as directed flow for p, *Σ, Λ* and antiflow for ***K-antiΣ-,antip-antiΛ,***

higher polarization for anti-Λ than for Λ

Back-up Slides

Single-particle method for extraction T-μB-μS

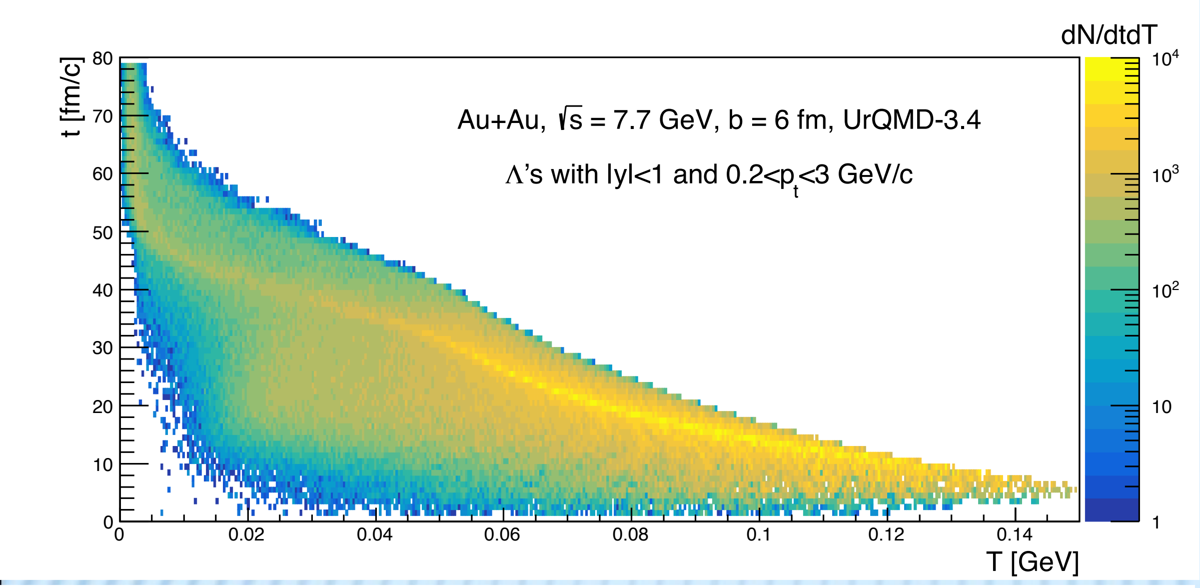

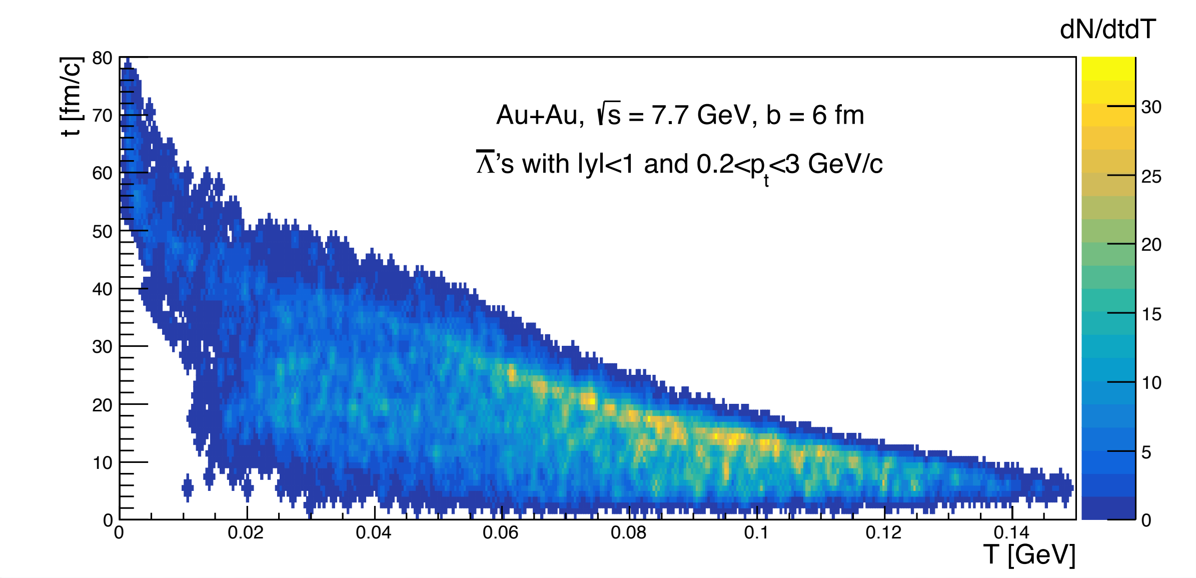

gives more precise estimation of average T-μ_B-μ_S

Thermal Approach

In local thermal equilibrium, the ensemble average of the spin vector for spin-1/2 fermions with four-momentum p at space-time point x is obtained from the statistical-hydrodynamical model as well as the Wigner function approach and reads

$$S^\mu(x,p) = -\frac{1}{8m}(1-n_F)\,\epsilon^{\mu\nu\rho\sigma} p_\nu \varpi_{\rho\sigma}(x),$$

where the thermal vorticity tensor is given by

$$\varpi_{\mu\nu} = \frac{1}{2}(\partial_\nu \beta_\mu - \partial_\mu \beta_\nu),$$

with $\beta^\mu = u^\mu / T$ being the inverse-temperature four-velocity. The number density of Λ's is very small so that we can make the approximation $1 - n_F \simeq 1$ Therefore:

$$S^\mu(x,p) = -\frac{1}{8m}\epsilon^{\mu\nu\rho\sigma} p_\nu \varpi_{\rho\sigma}(x).$$

By decomposing the thermal vorticity into the following components,

$$\boldsymbol{\varpi}_T = (\varpi_{0x}, \varpi_{0y}, \varpi_{0z}) = \frac{1}{2}\left[\nabla\left(\frac{\gamma}{T}\right) + \partial_t\left(\frac{\gamma\mathbf{v}}{T}\right)\right],$$

$$\boldsymbol{\varpi}_S = (\varpi_{yz}, \varpi_{zx}, \varpi_{xy}) = \frac{1}{2}\nabla\times\left(\frac{\gamma\mathbf{v}}{T}\right),$$

Equation can be rewritten as

$$S^0(x,p) = \frac{1}{4m}\mathbf{p}\cdot\boldsymbol{\varpi}_S, \quad \mathbf{S}(x,p) = \frac{1}{4m}\left(E_p\boldsymbol{\varpi}_S + \mathbf{p}\times\boldsymbol{\varpi}_T\right),$$

where E_p, $\mathbf{p}$, m are the Λ's energy, momentum, and mass, respectively.The spin vector of Λ in its rest frame is denoted as $S^{*\mu} = (0, \mathbf{S}^*)$ and is related to the same quantity in the c.m. frame by a Lorentz boost. Finally:

$$P = \frac{\langle\mathbf{S}^*\rangle\cdot\mathbf{J}}{|\langle\mathbf{S}^*\rangle||\mathbf{J}|},$$

[F. Becattini et al, Phys. Rev. C 95, 054902 (2017)]

UrQMD

- Represents a Monte Carlo method for the time evolution of the various phase space densities of particle species.
- Based on the covariant propagation of all hadrons on classical trajectories, stochastic binary scatterings, resonance and string formation with their subsequent decay.
- Provides the solution of the relativistic Boltzmann equation.
- The collision criterion (black disk approximation):
  $d < d_0 = \sqrt{\sigma_{tot}(\sqrt{s}, \text{type})/\pi}$
- 55 baryons and 32 mesons are included. All antiparticles and isospin-projected states are implemented.
- Cross sections are taken from PDG.
- Resonances are implemented in Breit–Wigner form.

[S. A. Bass et al, Prog. Part. Nucl. Phys. 41 (1998) 255-369,
M. Bleicher et al, J. Phys. G: Nucl. Part. Phys. 25 (1999) 1859-1896]

Statistical model

Input from UrQMD:

$$\varepsilon_{UrQMD} = \frac{1}{V}\sum_i E_i$$
$$\rho B_{UrQMD} = \frac{1}{V}\sum_i B_i$$
$$\rho S_{UrQMD} = \frac{1}{V}\sum_i S_i$$

Stat. Physics:

$$\varepsilon_{stat} = \sum_i \varepsilon_i(T, \mu_B, \mu_S)$$
$$\rho B_{stat} = \sum_i B_i n_i(T, \mu_B, \mu_S)$$
$$\rho S_{stat} = \sum_i S_i n_i(T, \mu_B, \mu_S)$$

$$\chi^2 = \frac{(\varepsilon_{UrQMD} - \varepsilon_{stat})^2}{\sigma_\varepsilon^2} + \frac{(\rho B_{UrQMD} - \rho B_{stat})^2}{\sigma_{\rho B}^2} + \frac{(\rho S_{UrQMD} - \rho S_{stat})^2}{\sigma_{\rho S}^2}$$

Minuit2 numerical minimizer

Output:
T, μ_B, μ_S

[L. Bravina et al, Phys. Rev. C60 (1999) 024904]